



Excitation-inhibition imbalance in medial preoptic area circuits underlies chronic stress-induced depression-like states

Received: 8 January 2024

Can Tao ^{1,4}, Guang-Wei Zhang ^{1,4}, Wen-Jian Sun¹, Junxiang J. Huang ^{1,2}, Li I. Zhang ^{1,3} & Huizhong Whit Tao ^{1,3}

Accepted: 18 September 2024

Published online: 03 October 2024

Check for updates

Dysregulation of brain homeostasis is associated with neuropsychiatric conditions such as major depressive disorder. However, underlying neural-circuit mechanisms remain not well-understood. We show in mice that chronic restraint stress (CRS) and social defeat stress (SDS) are both associated with disruption of excitation (E)-inhibition (I) balance, with increased E/I ratios, in medial preoptic area (MPOA) circuits, but through affecting different neuronal types. CRS results in elevated activity in glutamatergic neurons, and their suppression mitigates CRS-induced depressive-like behaviors. Paraventricular hypothalamic input to these neurons contributes to induction but not expression of depressive-like behaviors. Their projections to ventral tegmental area and periaqueductal gray/dorsal raphe suppress midbrain dopaminergic and serotonergic activity, respectively, and mediate expression of divergent depressive-like symptoms. By contrast, SDS results in reduced activity of GABAergic neurons, and their activation alleviates SDS-induced depressive-like behaviors. Thus, E/I imbalance with relatively increased excitation in MPOA circuits may be a general mechanism underlying depression caused by different etiological factors.

Dysregulations of the balance between neuronal excitation (E) and inhibition (I) in various brain regions are thought to play a critical role in neuropsychiatric disorders^{1,2}. Initially postulated as a mechanism underlying autism spectrum disorders³, the E-I imbalance subsequently has emerged as a potential brain circuit mechanism for a range of other mental disorders^{4,5} including the major depressive disorder (MDD)⁶, highlighting its relevance in mediating psychiatric illnesses.

MDD affects millions of people and is becoming one of the leading causes of disability worldwide⁷. Despite significant efforts devoted to understanding MDD, the limitations of current treatments, such as the slow antidepressant effects of selective serotonin reuptake inhibitors (SSRIs), underscores the need for exploring new therapeutic targets.

Accumulative evidence suggests that alterations in glutamate and GABA homeostasis may contribute critically to MDD pathology. This is supported by several key observations. First, alterations in glutamate and GABA levels have been reported in patients with MDD, characterized by elevated glutamate or deficient GABA⁶. Second, the association between MDD and epilepsy suggests potential hyperexcitatory states of neuronal networks in MDD⁸. Thirdly, medications targeting glutamate or GABA receptors, e.g., ketamine and brexanolone, exhibit fast and effective antidepressant effects, particularly in cases resistant to conventional treatments^{9–11}. However, the exact nature of E-I interactions contributing to depression remains elusive. It is also unclear whether various etiologies for depression differentially impact excitatory and inhibitory neuronal populations.

¹Zilkha Neurogenetic Institute and Center for Neural Circuits and Sensory Processing Disorders, Keck School of Medicine, University of Southern California, Los Angeles, CA 90033, USA. ²Graduate Program in Biological and Biomedical Sciences, Keck School of Medicine, University of Southern California, Los Angeles, CA 90033, USA. ³Department of Physiology and Neuroscience, Keck School of Medicine, University of Southern California, Los Angeles, CA 90033, USA. ⁴These authors contributed equally: Can Tao, Guang-Wei Zhang. e-mail: liizhang@usc.edu; htao@usc.edu

The MPOA is located at the anterior part of the hypothalamus and is composed of glutamatergic and GABAergic neuronal populations¹², which appear to function antagonistically. For example, the GABAergic population encodes positive valence¹³, promotes parental behavior^{14,15} and social interactions^{16,17}, generates anxiolytic effects¹³ and increases food intake¹⁸. Moreover, it mediates the depressive-like state in female mice following ovarian hormone withdrawal via connectivity (direct or indirect) to midbrain monoaminergic systems¹⁹. The glutamatergic population, on the other hand, encodes negative valence, suppresses parental behavior and mediates anxiety-like states induced by acute stressors¹³. These results suggest that a dysregulation of E-I balance in the MPOA circuit might contribute to the multifaceted behavioral deficits in depressive-like states^{12,13,16-19}. However, it remains unclear whether these two distinct neuronal populations in the MPOA respond differently under various stress conditions that lead to depressive-like states, such as chronic restraint and social defeat stresses. Additionally, the potential involvement of E-I interplay within the MPOA-midbrain circuits in regulating depressive-like behaviors remains undetermined.

In this study, we found that chronic restraint stress (CRS) resulted in increased baseline firing activity, specifically in the glutamatergic neurons of MPOA. Silencing of these neurons had an acute anti-depressant effect. In addition, excitatory projections from the paraventricular hypothalamic nucleus (PVH) to the MPOA glutamatergic neurons were critical for the induction but not expression of the stress-induced depressive-like behaviors. Moreover, the MPOA glutamatergic neurons projected to the ventral tegmental area (VTA) and ventrolateral periaqueductal gray (vlPAG), and suppressed activity of VTA dopaminergic and DR serotonergic neurons, respectively. By contrast, under chronic social defeat stress (SDS), a decrease of MPOA GABAergic activity, without a change of glutamatergic activity, was observed. Activation of the GABAergic population alleviated the SDS-induced depressive-like behaviors. Our results suggest that different stress types differentially impact glutamatergic and GABAergic MPOA neurons, nonetheless leading to a universal increase in the E-I ratio at the MPOA output. Overall, our study suggests that maladaptation of the E-I balance in MPOA-midbrain circuits under stress conditions may represent a common underlying cause for the development of depressive-like states.

Results

Hyperactivity of MPOA glutamatergic neurons following chronic restraint stress

To induce depressive-like states, we employed a well-established CRS model for rodents²⁰ (see "Methods" for details). Mice subjected to 3 weeks of daily body restraint for 2 h per day (Fig. 1a) displayed a variety of depressive-like behaviors, as measured by a battery of behavioral tests (Fig. 1b-g). These tests included the sucrose preference test (SPT) for assessing anhedonia, tail suspension test (TST) and forced swimming test (FST) for measuring immobility, social preference test for evaluating sociability, and elevated plus maze (EPM) test and open field test (OFT) for assessing anxiety-like behavior. Behaviors were scored automatically (Supplementary Fig. 1a-f). Compared to control animals that experienced similar handling without body restraint, the CRS-treated mice showed diminished sucrose preference in SPT (Fig. 1b), heightened immobility in TST and FST (Fig. 1c, d), reduced social preference (Fig. 1e), and decreased time spent in the open arms of EPM and in the central area of OFT (Fig. 1f, g). Male and female mice demonstrated similar behavioral deficits (Supplementary Fig. 1g-l). Moreover, CRS-treated virgin female mice displayed reduced pup grooming (i.e., reduced parenting), and CRS-treated male mice showed diminished mounting behavior (Supplementary Fig. 1m, n).

To investigate cell-type specific neural activity changes in the MPOA following CRS treatment, we conducted optrode recordings^{21,22}

from channelrhodopsin-2 (ChR2) tagged glutamatergic and GABAergic neurons in awake *Vglut2-Cre:Ai27* and *Vgat-Cre:Ai27* mice, respectively (Fig. 1h-j). We selected *Slc17a6* (*Vglut2*) and *Slc32a1* (*Vgat*) as they are the two most definitive molecular markers for distinguishing glutamatergic and GABAergic neuron populations in MPOA¹². We found that the baseline firing activity of glutamatergic neurons was significantly higher in CRS-treated mice compared to control animals (Fig. 1k, l). In the meanwhile, we noticed a substantial increase in the number of cells exhibiting burst-firing patterns in the glutamatergic population of CRS-treated mice compared to control animals (Fig. 1m, n). By contrast, the recorded GABAergic neurons did not display a significant alteration in the baseline firing rate or firing pattern (Fig. 1o-q). These observations suggest that CRS specifically results in hyperactivity of glutamatergic but not GABAergic neurons in the MPOA. As such, the E/I balance of the MPOA circuit has been changed in that the E/I ratio is increased.

To examine the progression of the MPOA glutamatergic neuron hyperactivity during CRS treatment, we monitored Ca²⁺ signals of individual neurons using miniscope imaging (see "Methods"). To this end, we injected adeno-associated virus (AAV) encoding Cre-dependent GCaMP7s into MPOA of *Vglut2-Cre* mice (Supplementary Fig. 2a). After segmentation and alignment of all collected cells (Supplementary Fig. 2b-d), we found an increase in the frequency of spontaneous Ca²⁺ transients at the population level (Supplementary Fig. 2e), detectable after about 1 week of stress exposure and gradually heightened till the end of CRS treatment (Supplementary Fig. 2f). In the meantime, we were able to trace 7 cells throughout the entire CRS period (Supplementary Fig. 2d, e), and the progressively heightened activity was confirmed in these individual neurons (Supplementary Fig. 2g). These observations indicate a gradual development of hyperactivity of MPOA glutamatergic neurons during CRS treatment.

Cellular changes associated with the hyperactivity of MPOA glutamatergic neurons

To investigate whether the elevated firing activity of MPOA glutamatergic neurons *in vivo* could be attributed to changes in intrinsic membrane properties, we performed whole-cell patch clamp recordings in brain slices prepared from CRS-treated and control *Vglut2-Cre:Ai14* mice (Fig. 2a). In recorded tdTomato-labeled glutamatergic neurons, we noticed a significant increase in the spontaneous spike rate (Fig. 2b) and a larger percentage of cells displaying burst-firing patterns in CRS than control slices (Fig. 2c). To evaluate intrinsic excitability, we injected square currents of varying amplitudes into the recorded cell (Fig. 2d). In control neurons, the number of spikes evoked by a depolarizing current injection reached a plateau and then decreased with increasing current amplitudes (Fig. 2e, black), due to depolarization block (Fig. 2d). On the other hand, in CRS neurons, the number of evoked spikes monotonically increased with increasing current amplitudes and became much higher than that of control neurons at high current amplitudes (Fig. 2e, red). Moreover, the frequency and amplitude of spontaneous excitatory postsynaptic currents (sEPSCs) in the MPOA glutamatergic neuron significantly increased in CRS compared to control slices (Fig. 2f-h), while the spontaneous inhibitory postsynaptic currents (sIPSCs) did not exhibit a significant change in either frequency or amplitude (Fig. 2i-k). In comparison, GABAergic neurons selectively recorded in slices from *Vgat-Cre:Ai14* mice displayed no significant differences in excitability or synaptic activity between CRS and control groups (Fig. 2l-r), indicating that the cellular changes in CRS animals are specific to the glutamatergic population, which corroborates the *in vivo* observations of firing rates in these two distinct cell types. Collectively, our results suggest that the observed hyperactivity of MPOA glutamatergic neurons can be attributed, at least partially, to changes in intrinsic membrane properties and excitatory synaptic input of these neurons.

MPOA glutamatergic activity is required for both induction and expression of depressive-like behaviors

We next examined whether the hyperactivity of MPOA glutamatergic neurons could contribute to the depressive-like behaviors observed in CRS mice by suppressing their activity. To this end, we expressed Cre-dependent inhibitory DREADD receptor, hM4Di (or mCherry as control), in MPOA glutamatergic neurons of *Vglut2-Cre* mice (Fig. 3a, Supplementary Fig. 3a–c). Silencing these neurons by CNO administration (for timeline see Supplementary Fig. 3d) during the expression phase (i.e., after CRS treatment) ameliorated depressive-like behaviors, as shown by the increased sucrose preference (Fig. 3b), diminished immobility (Fig. 3c, d), reduced anxiety-like behavior (Fig. 3e, f), as well as increased social preference (Fig. 3g) as compared to mCherry control animals. As control, the chemogenetic inhibition of MPOA glutamatergic neurons in mice not exposed to stress did not generate a significant effect on any of the tested behaviors (Supplementary Fig. 4).

Next, we examined the impact of suppressing MPOA glutamatergic activity during the induction phase, by daily administrating CNO

before stress exposure throughout the CRS period (Fig. 3h). We found that chronically suppressing MPOA glutamatergic neurons during the induction phase prevented the development of depressive-like behaviors, as shown by the increased sucrose preference (Fig. 3i), diminished immobility (Fig. 3j, k), reduced anxiety-like behavior (Fig. 3l, m), as well as increased social preference (Fig. 3n) as compared to mCherry control animals. Together, our data suggest that MPOA glutamatergic activity is required for both the induction and expression of depressive-like behaviors.

PVH→MPOA projection is necessary for the induction but not expression of depressive-like behaviors

MPOA glutamatergic neurons receive inputs from several upstream structures that can respond to stress¹³. Among these, we identified the PVH as the most prominent source of excitatory input to MPOA, using retrograde tracing in combination with RNAscope staining for *Vglut2* and Cre (Fig. 4a–c). This finding is in line with previous anatomical results²³. Notably, nearly all (92.4%) of PVH neurons projecting to MPOA were glutamatergic. To determine whether corticotropin-

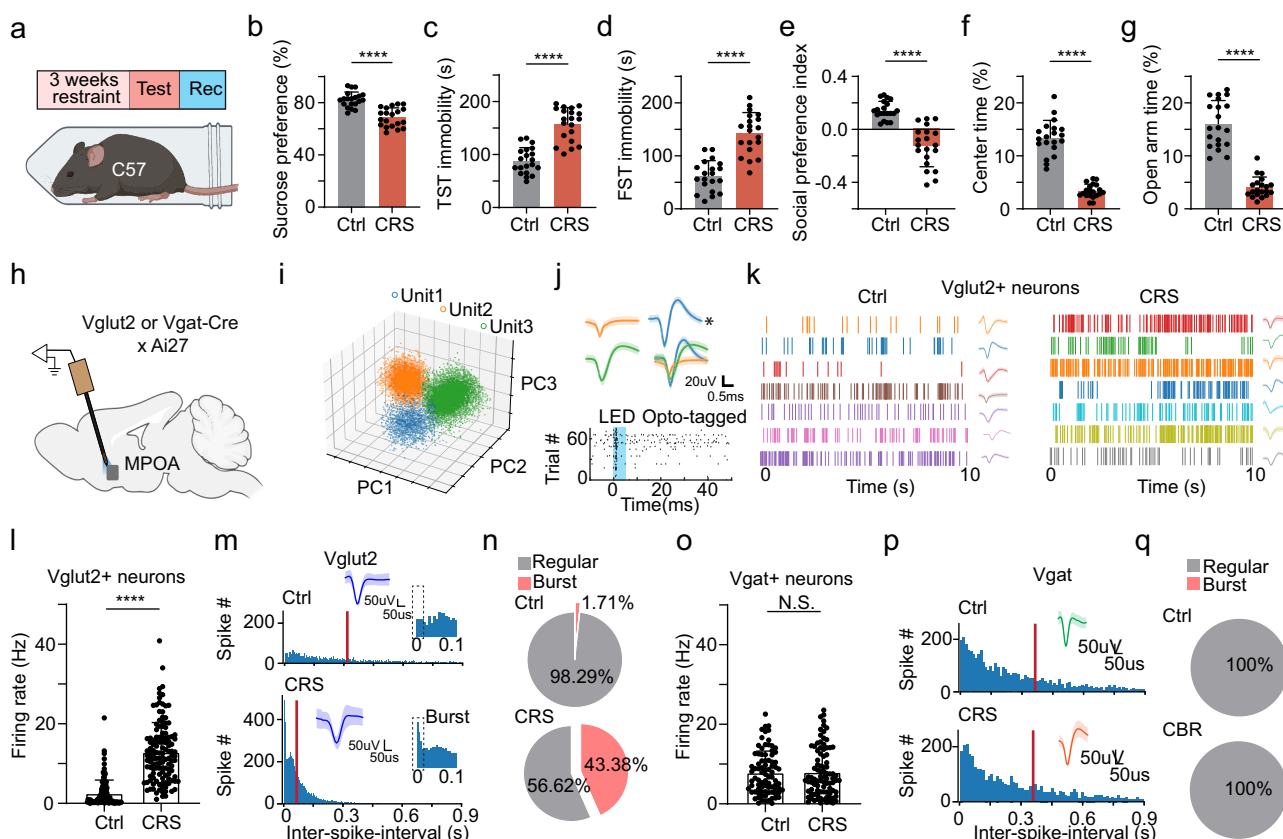


Fig. 1 | Enhanced glutamatergic activity in MPOA following chronic restraint stress. **a** Schematic of chronic restraint stress. **b** Percentage sucrose water consumption. Ctrl control, CRS chronic restraint stress. **c** Immobility time in tail suspension test (TST). **d** Immobility time in forced swimming test (FST). **e** Social preference index (difference in time between two chambers divided by the total time) in the three-chamber sociability test. **f** Percentage time spent in the center in the open field test (OFT). **g** Percentage time spent in opened arms of elevated plus maze (EPM). **b–g** $****p < 0.0001$, two-tailed unpaired t -test, $n = 20$ mice in each group. Data are presented as mean \pm s.d. **h** Schematic of optrode recording in MPOA of *Vgat-Cre::Ai27* or *Vglut2-Cre::Ai27* mouse. **i** Example spike sorting. Each dot represents one spike event. Different colors label different units. **j** Upper, average spike shapes of the three units shown in (i). Lower, raster plot for spikes evoked by LED light pulses (blue shade, 5-ms) in a ChR2-tagged unit. **k** Raster plots of spontaneous spikes for seven *Vglut2*⁺ neurons in control (left) and CRS (right) animals. Right insets are superimposed spike waveforms for each unit. **l** Firing rates

of all the recorded *Vglut2*⁺ neurons in control and CRS groups ($n = 116$ and 127 cells, respectively, from three animals in each group). $****p < 0.0001$, two-tailed unpaired t -test. **m** Distributions of inter-spike intervals (ISIs) for two example *Vglut2*⁺ neurons in a control (top) and CRS (bottom) animal. Red vertical line indicates the median value. Inset, superimposed spike waveforms and zoomed-in histogram within 0–100 ms range, with two dashed vertical lines mark ISIs for bursting firing. **n** Pie chart showing the percentage of bursting firing cells in *Vglut2*⁺ neurons in control (top) and CRS (bottom) animals. **o** Spike rates of all the recorded ChR2-tagged *Vgat*⁺ neurons in control and CRS groups ($n = 84$ and 89 cells, respectively, from three animals in each group). N.S., $p = 0.8931$, two-tailed unpaired t -test. **p** Distributions of ISIs for example *Vgat*⁺ cells in control and CRS animals. **q** Pie chart for the percentage of bursting firing cells in *Vgat*⁺ neurons. All error bars represent s.d. For exact p values, see Source Data. **(a)** and **(h)** were created with BioRender.com.

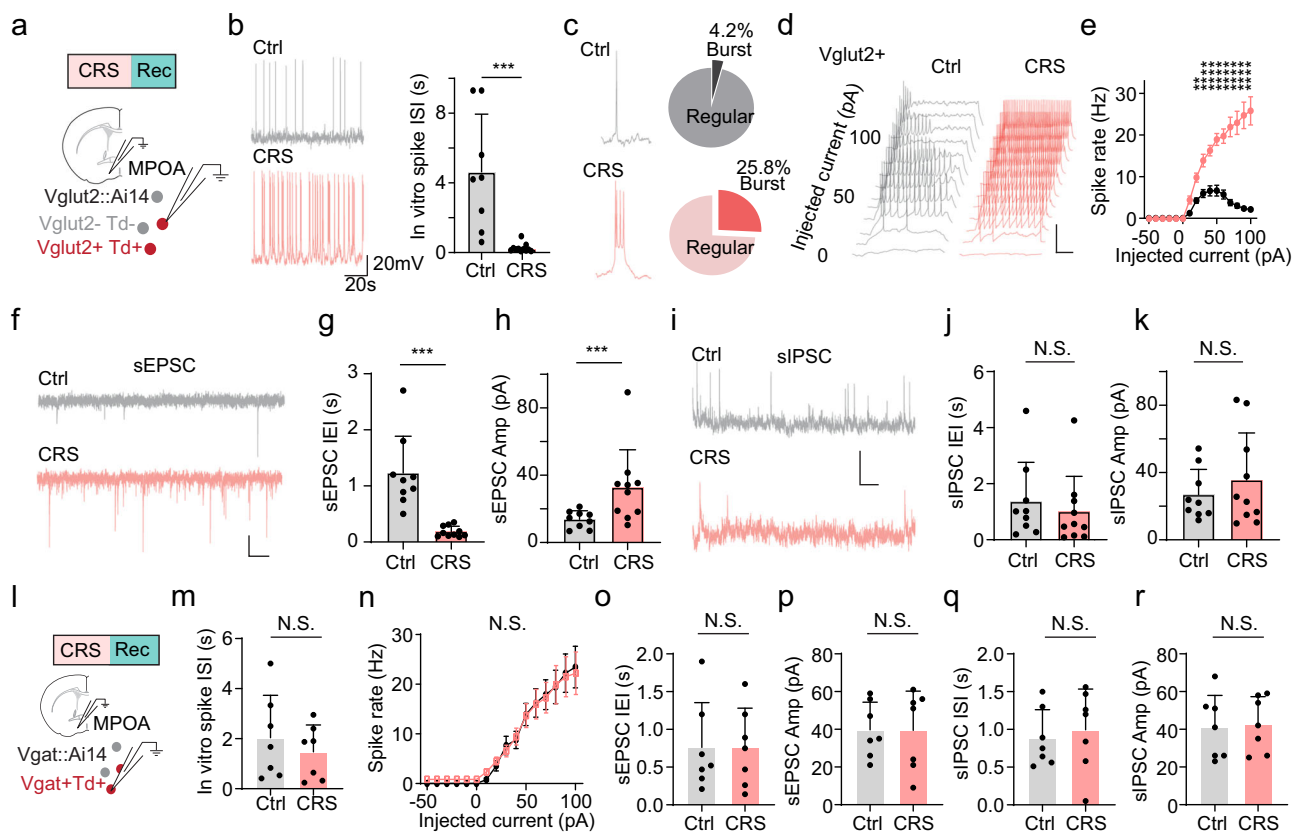


Fig. 2 | Cellular changes associated with hyperactivity of MPOA glutamatergic neurons. **a** Schematic whole-cell recording from MPOA Vglut2+ neurons in slice preparations. **b** Left, example recorded traces of spontaneous spikes from a control (gray) and CRS (red) neuron. Right, mean ISIs in control and CRS groups ($n=10$ and 10 cells, respectively, from three animals in each group). *** $p=0.0044$, two-tailed Mann-Whitney test. **c** Left, trace of bursting firing in an example Vglut2+ neuron. Right, percentage of bursting firing cells. **d** Membrane potential responses to step-current injections in a control (gray) and CRS (red) neuron. Scale: 50 mV, 200 ms. **e** Average input-output function of Vglut2+ neurons in control and CRS groups ($n=9$ and 10 cells, respectively, from three animals in each group)). ** $p<0.01$, *** $p<0.0001$, two-tailed repeated measures two-way ANOVA with Sidak's test. **f** Recorded traces of sEPSCs in example Vglut2+ neurons in control (gray) and CRS (red) slices. Scale: 20 pA, 200 ms. **g, h** Mean inter-event intervals (g, IEIs) and mean amplitudes (h) of sEPSCs in control and CRS slices ($n=9$ and 10 cells, respectively, from three animals in each group). **** $p<0.0001$ (g) and ** $p=0.007$ (h), two-tailed Mann-Whitney test. **i-k** Similar to (f-h) but for sIPSCs ($n=9$ and 10 cells for control and CRS, respectively, from three animals in each group). Scale: 20 mV, 200 ms. N.S., $p=0.3154$ (j) and $p=0.8421$ (k), two-tailed Mann-Whitney test. **l** Whole-cell recording from MPOA Vgat+ neurons. **m** Mean ISIs of Vgat+ neurons in control and CRS groups ($n=7$ and 7 cells, respectively, from two animals in each group). N.S., $p=0.535$, two-tailed Mann-Whitney test. **n** Average input-output function of Vgat+ neurons in control and CRS groups ($n=7$ and 7 cells, respectively, from three animals in each group). $p=0.5337$, two-tailed repeated measures two-way ANOVA. **o, p** Mean IEIs (o) and amplitudes (p) of sEPSCs in Vgat+ neurons in control and CRS slices ($n=7$ and 7 cells, respectively, from three animals in each group). N.S., $p=0.9802$ (o) and $p=0.9767$ (p), two-tailed Mann-Whitney test. **q, r** Similar to (o, p) but for sIPSCs ($n=7$ and 7 cells for control and CRS, respectively, from three animals in each group). N.S., $p=0.62$ (q) and $p=0.71$ (r), two-tailed Mann-Whitney test. Error bar represents s.d. in (b), (g, h), (j, k), (o-r) and s.e.m. in (e), (n). For exact p values, see Source Data.

Mann-Whitney test. **i-k** Similar to (f-h) but for sIPSCs ($n=9$ and 10 cells for control and CRS, respectively, from three animals in each group). Scale: 20 mV, 200 ms. N.S., $p=0.3154$ (j) and $p=0.8421$ (k), two-tailed Mann-Whitney test. **l** Whole-cell recording from MPOA Vgat+ neurons. **m** Mean ISIs of Vgat+ neurons in control and CRS groups ($n=7$ and 7 cells, respectively, from two animals in each group). N.S., $p=0.535$, two-tailed Mann-Whitney test. **n** Average input-output function of Vgat+ neurons in control and CRS groups ($n=7$ and 7 cells, respectively, from three animals in each group). $p=0.5337$, two-tailed repeated measures two-way ANOVA. **o, p** Mean IEIs (o) and amplitudes (p) of sEPSCs in Vgat+ neurons in control and CRS slices ($n=7$ and 7 cells, respectively, from three animals in each group). N.S., $p=0.9802$ (o) and $p=0.9767$ (p), two-tailed Mann-Whitney test. **q, r** Similar to (o, p) but for sIPSCs ($n=7$ and 7 cells for control and CRS, respectively, from three animals in each group). N.S., $p=0.62$ (q) and $p=0.71$ (r), two-tailed Mann-Whitney test. Error bar represents s.d. in (b), (g, h), (j, k), (o-r) and s.e.m. in (e), (n). For exact p values, see Source Data.

releasing hormone (CRH) positive neurons give rise to this projection, we injected AAVretro-Cre in MPOA and performed RNAscope staining for Cre and CRH in PVH (Fig. 4d, e). We found that the MPOA-projecting PVH neurons were predominantly non-CRH-positive (Fig. 4f). In *Vglut2-Cre:Ai14* animals, we expressed Cre-dependent ChR2 in the PVH and conducted whole-cell patch clamp recordings from tdTomato-labeled glutamatergic and unlabeled presumptive GABAergic neurons in the MPOA (Fig. 4g). PVH glutamatergic axons were found to innervate the glutamatergic population in the MPOA much more strongly than the GABAergic population (Fig. 4h, i). These anatomical and functional connectivity studies suggest that the excitatory projection from PVH to MPOA glutamatergic neurons may provide stress signals to drive plastic changes in the latter cells.

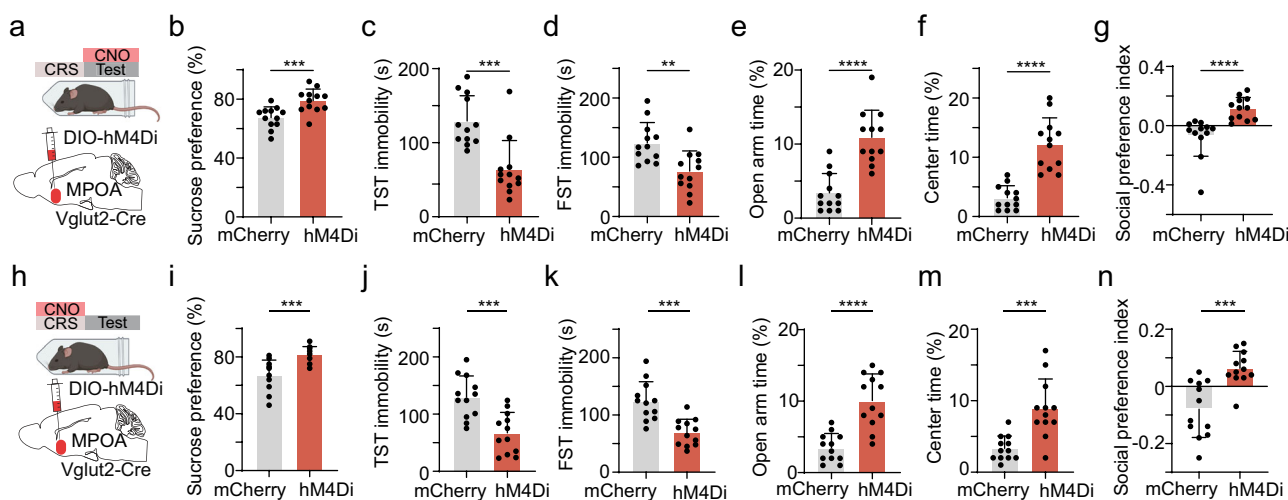
We thus examined the role of MPOA-projecting PVH neurons in the induction of depressive-like behaviors. We targeted these neurons by injecting AAVretro-Cre in MPOA and AAV encoding Cre-dependent hM4Di in PVH (Fig. 4j). CNO was administered daily throughout the CRS period. After completing the CRS treatment, we observed significant differences in sucrose preference (Fig. 4k), immobility

(Fig. 4l, m), anxiety-related behavior (Fig. 4n, o) and social preference (Fig. 4p) compared to mCherry controls. These results suggest that the activity of MPOA-projecting PVH glutamatergic neurons is required for the induction of depressive-like behaviors by CRS treatment.

Next, we investigated the involvement of MPOA-projecting PVH neurons in the expression phase of depressive-like behaviors by administering CNO post CRS treatment (Fig. 4q). Surprisingly, we did not observe a significant change in sucrose preference (Fig. 4r), immobility (Fig. 4s, t), anxiety-related behavior (Fig. 4u, v) or social preference (Fig. 4w) as compared to mCherry control. This indicates that the PVH→MPOA projection is not required for the expression of depressive-like behaviors. Moreover, we chemogenetically silenced MPOA-projecting LHA neurons and found that they were not involved in the expression of depressive-like behaviors either (Supplementary Fig. 5).

Distinct MPOA^{Vglut2} projections mediate different depressive-like symptoms

How does the hyperactivity of the MPOA glutamatergic population result in depressive-like behaviors? Previous studies, including our



own, have demonstrated that both MPOA glutamatergic and GABAergic neurons project to VTA as well as vIPAG^{13,19,24}, results of which have been replicated in the current study (Supplementary Fig. 6). We thus separately investigated the involvement of long-range MPOA projections to VTA and vIPAG.

To investigate how MPOA glutamatergic neurons might modulate neuronal activity in VTA, we directly recorded from dopamine (DA) and non-DA neurons in VTA while optogenetically activating MPOA glutamatergic neurons in awake head-fixed animals (see “Methods”). To this end, we injected AAV-fDIO-ChR2 into MPOA and AAV-DIO-ChrimsonR into VTA of *Vglut2-Flp::Dat-Cre* mice (Fig. 5a). Optrode recordings were performed in VTA to identify ChrimsonR-tagged dopaminergic (Dat+) neurons (with red light activation) and record their responses to the activation of MPOA glutamatergic neurons (by blue light). We observed that the activation of MPOA glutamatergic neurons significantly increased and decreased firing rates in 5% and 41% of the identified Dat+ neurons, respectively (Fig. 5b, d, e). In comparison, in the non-tagged group, 29% were observed to increase their firing rates upon activation of MPOA glutamatergic neurons, while 9% were suppressed (Fig. 5c, d, f). These data demonstrate a net suppressive effect on DA neurons by activating MPOA glutamatergic neurons.

Next, we specifically investigated the role of MPOA→VTA glutamatergic projections in depressive-like behaviors by expressing Cre-dependent halorhodopsin (eNpHR3.0)^{25–27} in MPOA of CRS-treated *Vglut2-Cre* mice and applying light stimulation via implanted optic fibers above VTA (Fig. 5g). Suppressing the MPOA^{Vglut2}→VTA terminals did not significantly affect immobility or anxiety-like behavior, but increased sucrose preference and social preference compared to GFP control animals (Fig. 5h–m).

Since MPOA glutamatergic axons terminate in the PAG regions surrounding the dorsal raphe (DR)¹³, one major area containing serotonergic neurons²⁸, we examined whether MPOA glutamatergic neurons could modulate DR serotonergic activity. AAV-fDIO-ChR2 was injected into MPOA and AAV-DIO-ChrimsonR into DR of *Vglut2-Flp::Sert-Cre* mice (Fig. 5n). Optrode recording was performed in vIPAG/DR regions to identify serotonergic (Sert+) neurons (with red light activation) and record their responses to the activation of MPOA

glutamatergic neurons (by blue light). We found that in the identified Sert+ neurons, 6.8% and 26.1% exhibited a significant increase and decrease in firing rate, respectively, upon the activation (Fig. 5o, q, r). In the non-tagged neurons, 11% decreased, and 30% increased their firing rates (Fig. 5p, q, s). Thus, our data demonstrate that MPOA glutamatergic activity overall suppresses midbrain dopaminergic as well as serotonergic activity. We then optogenetically suppressed the MPOA^{Vglut2}→vIPAG terminals after CRS treatment (Fig. 5t). This did not noticeably affect sucrose preference but reduced immobility, anxiety-like behavior, as well as social preference (Fig. 5u–z). Together, our data suggest distinct functional roles of VTA-projecting and PAG-projecting MPOA neurons, which are essentially separate populations^{13,19}: while both the MPOA glutamatergic projections contribute to social withdrawal, the one directed to vIPAG primarily mediates the behavioral despair and anxiety, whereas the one directed to VTA predominantly mediates the anhedonia aspect of CRS-induced depressive-like symptoms.

Chronic social defeat stress decreases MPOA GABAergic activity
We have shown that the E/I balance in MPOA circuits is altered following chronic restraint stress. We wondered if this could be generalized to other stress conditions. To test this idea, we used a well-documented chronic social defeat stress (SDS) model^{29,30} (Fig. 6a, see “Methods”). Following a 10-day exposure to SDS, approximately 80% of the tested animals demonstrated robust depressive-like behaviors (Fig. 6b–g).

To assay the E/I balance in MPOA of the SDS-treated depressive mice, we conducted *in vivo* optrode recordings from opto-tagged Vgat+ or Vglut2+ neurons after verifying the expression of depressive-like behaviors (Fig. 6h). Intriguingly, we observed significant alterations in the Vgat+ but not the Vglut2+ neurons of SDS animals compared to control mice without SDS exposure (Fig. 6i–l). Specifically, the GABAergic neurons exhibited reduced spontaneous firing rates (Fig. 6i–k). Whole-cell patch clamp recording from brain slices (Fig. 6m) also revealed reduced intrinsic membrane excitability of the GABAergic neurons, as shown by the altered input–output function, with the glutamatergic neurons spared (Fig. 6n–q). On the other hand, sEPSCs and sIPSCs were apparently not affected in either the Vglut2+

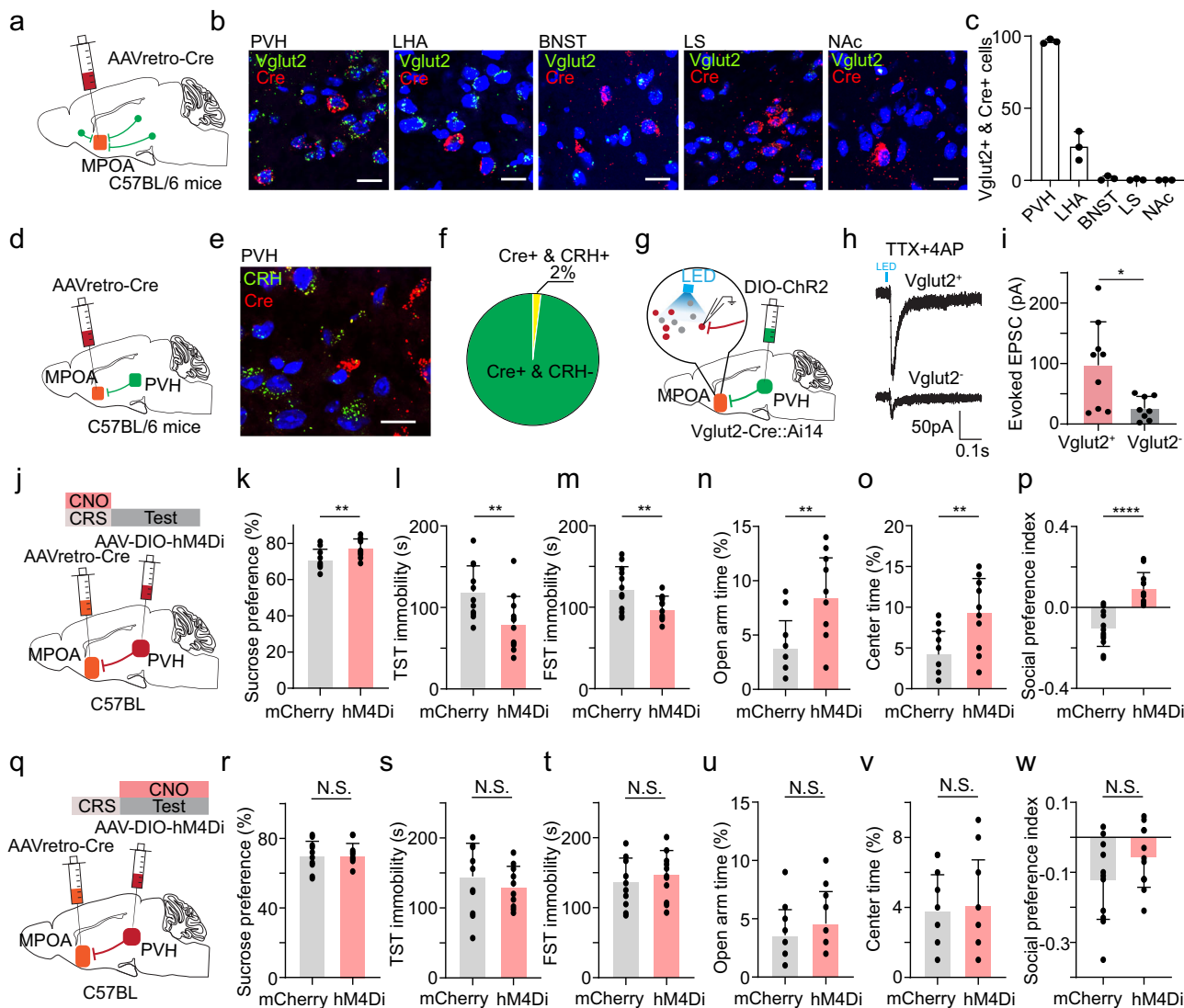


Fig. 4 | Excitatory PVH-MPOA projection is required for the induction but not expression of depressive-like behaviors. **a** Schematic of identifying glutamatergic neurons that project to MPOA. **b** Example images showing RNAscope staining of Vglut2 and Cre in PVH, LHA, BNST, LS and NAc. Scale bar: 20 μ m. **c** Numbers of double positive (Cre+ & Vglut2+) cells in different regions. $n = 3$ animals for each group. **d** Schematic of injection of AAVretro-Cre in MPOA. **e** RNAscope staining of CRH and Cre in PVH ($n = 3$ animals). Scale bar: 20 μ m. **f** Percentage of CRH and Cre double positive out of Cre+ cells. **g** Slice whole-cell recording of MPOA Vglut2+ or Vglut2- neurons in response to activation of PVH axon terminals. **h** Light-evoked EPSCs in example Vglut2+ and Vglut2- neurons, recorded at -70 mV and in the presence of TTX and 4-AP. **i** Average amplitudes of light-evoked EPSCs in MPOA Vglut2+ and Vglut2- population. * $p < 0.05$, two-tailed t -test. $n = 9$ cells from 3 animals.

j Schematic of viral injection and chemogenetic inhibition of MPOA-projecting PVH neurons during the induction phase. **k** Percentage sucrose water consumption in mCherry- or hM4Di-expressing CRS animals. **l** Immobility time in TST. **m** Immobility time in FST. **n** Percentage time spent in open arms in EPM test. **o** Percentage time spent in the center in OFT. **p** Social preference index. **k-p** $n = 12$ animals for each group. **q-w** Similar to (j-p) but for chemogenetic silencing of MPOA-projecting PVH neurons following CRS treatment ($n = 12$ animals for each group). Statistics for (k-w), N.S., $p \geq 0.05$, * $p < 0.05$, ** $p < 0.01$, *** $p < 0.001$ and **** $p < 0.0001$, two-tailed Mann-Whitney test. All error bars represent s.d. For exact p values, see Source Data.

or Vgat+ population (Supplementary Fig. 7a-h). Together, these data indicate that SDS treatment also results in an increase in E/I ratio, but by decreasing inhibitory activity.

We further investigated whether enhancing MPOA GABAergic activity could mitigate depressive-like behaviors following SDS treatment. To this end, we expressed a Cre-dependent excitatory DREADD receptor, hM3Dq, in MPOA of *Vgat-Cre* mice (Fig. 6r). The chemogenetic activation of the GABAergic neurons after SDS treatment significantly ameliorated depressive-like behaviors, evidenced by elevated sucrose preference, reduced immobility, diminished anxiety-like behavior and increased social preference as compared to mCherry mice (Fig. 6s-x). Optogenetic activation of the neurons generated similar effects (Supplementary Fig. 7i-o). As control, chemogenetically activation of Vgat+ neurons in mice not exposed to SDS did not

generate a significant effect on any of the tested behaviors (Supplementary Fig. 7p-v). Together, these data indicate that similar to the glutamatergic hyperactivity induced by CRS, the GABAergic hypoactivity induced by SDS can also lead to the expression of depressive-like behaviors.

Disrupting the MPOA E/I balance is sufficient for inducing depressive-like states

Our results have revealed a common disruption of the neuronal E/I balance in MPOA circuits using two different stress models. To understand whether the MPOA E/I balance is pivotal in regulating depressive-like states, we artificially manipulated this parameter. In CRS-treated mice, we chemogenetically (Fig. 7a) or optogenetically (Supplementary Fig. 8a) activated the GABAergic neurons to normalize

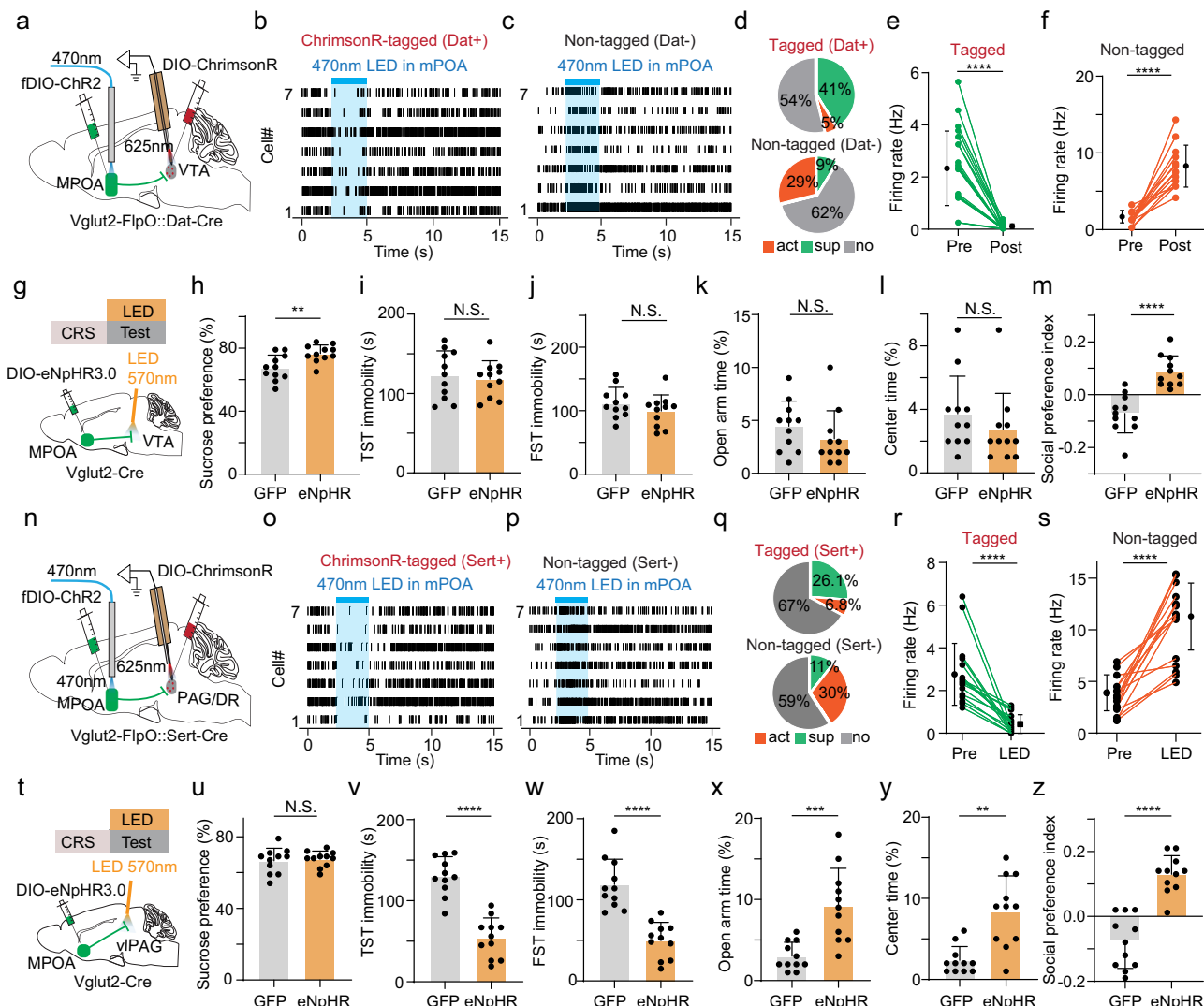


Fig. 5 | MPOA glutamatergic activity suppresses midbrain dopaminergic and serotonergic activity. **a** Schematic of recording from VTA Dat⁺ neurons tagged with ChrimsonR while photo-activating MPOA glutamatergic neurons *in vivo*. **b, c** Raster plots for seven opto-tagged (**b**, Dat⁺) and non-tagged (**c**) VTA neurons in response to activation of MPOA glutamatergic neurons. **d** Fractions of tagged and non-tagged VTA neurons showing different types of responses. **e** Firing rate changes for suppressed Dat⁺ neurons. $p < 0.0001$, two-tailed paired *t*-test, $n = 21$ cells. Bar represents s.d. **f** Firing rate changes of activated non-tagged neurons. $p < 0.0001$, two-tailed paired *t*-test, $n = 14$ cells. **g** Schematic of viral injection and optogenetic silencing of glutamatergic MPOA axon terminals in VTA in CRS animals. **h** Percentage sucrose water consumption in GFP- or eNpHR-expressing CRS animals. **i** Immobility time in TST. **j** Immobility time in FST. **k** Percentage time spent in open arms in EPM test. **l** Percentage time spent in the center in OFT. **m** Social preference index. **h–m** $n = 12$ animals for each group. ** $p < 0.01$,

*** $p < 0.0001$, two-tailed Mann–Whitney test. **n** Schematic of recording from PAG/DR Sert⁺ neurons tagged with ChrimsonR while photo-activating MPOA glutamatergic neurons. **o, p** Raster plots for seven tagged (**o**, Sert⁺) and non-tagged (**p**) PAG/DR neurons in response to activation of MPOA glutamatergic neurons. **q** Fractions of tagged and non-tagged PAG/DR neurons showing different types of responses. **r** Firing rate changes of suppressed tagged neurons. $p < 0.0001$, two-tailed paired *t*-test, $n = 17$ cells. **s** Firing rate changes of activated non-tagged neurons. $p < 0.0001$, two-tailed paired *t*-test, $n = 16$ cells. **t** Schematic of viral injection and optogenetic silencing of glutamatergic MPOA axon terminals in PAG/DR regions in CRS animals. **u–z** Similar to (**h–m**), but for optogenetic silencing of MPOA→PAG/DR axons. $n = 12$ animals for each group. ** $p < 0.01$, *** $p < 0.001$ and *** $p < 0.0001$, two-tailed Mann–Whitney test. All error bars represent s.d. For exact *p* values, see Source Data.

the E/I ratio by enhancing inhibitory activity. This acutely resulted in the alleviation of depressive-like behaviors (Fig. 7b–g, Supplementary Fig. 8b–g), similar to suppressing glutamatergic activity. Next, we tested whether chronically manipulating the E/I balance was sufficient for inducing persistent depressive-like behaviors, by chronically activating MPOA Vglut2⁺ neurons with chemogenetics (Fig. 7h). Compared to mCherry controls, daily injections of CNO in the hM3Dq-expressing animals for 2 weeks resulted in manifestations of depressive-like behaviors even when CNO wore out (Fig. 7i–n). In another set of experiments, we chronically inhibited the GABAergic neurons by expressing hM4Di (Fig. 7o). Similarly, daily administration of CNO for 2 weeks resulted in persistent expression of depressive-like

behaviors (Fig. 7p–u). These data indicate that chronically increasing the E/I ratio in MPOA circuits either by enhancing glutamatergic or by reducing GABAergic activity is sufficient for inducing persistent depressive-like states.

We wondered to what degree manipulations of one MPOA neuronal population would affect the other. To address this issue, we investigated local synaptic connections between MPOA Vgat⁺ and Vglut2⁺ neurons using slice recording. Cre-dependent ChR2 virus was injected in MPOA of *Vglut2-Cre:Ai14* and *Vgat-Cre:Ai14* mice, and selected whole-cell recording was made from Vglut2⁺ and Vgat⁺ neurons, respectively (Supplementary Fig. 9a, c). We found that the connection from Vglut2⁺ to Vgat⁺ neurons was at most very weak,

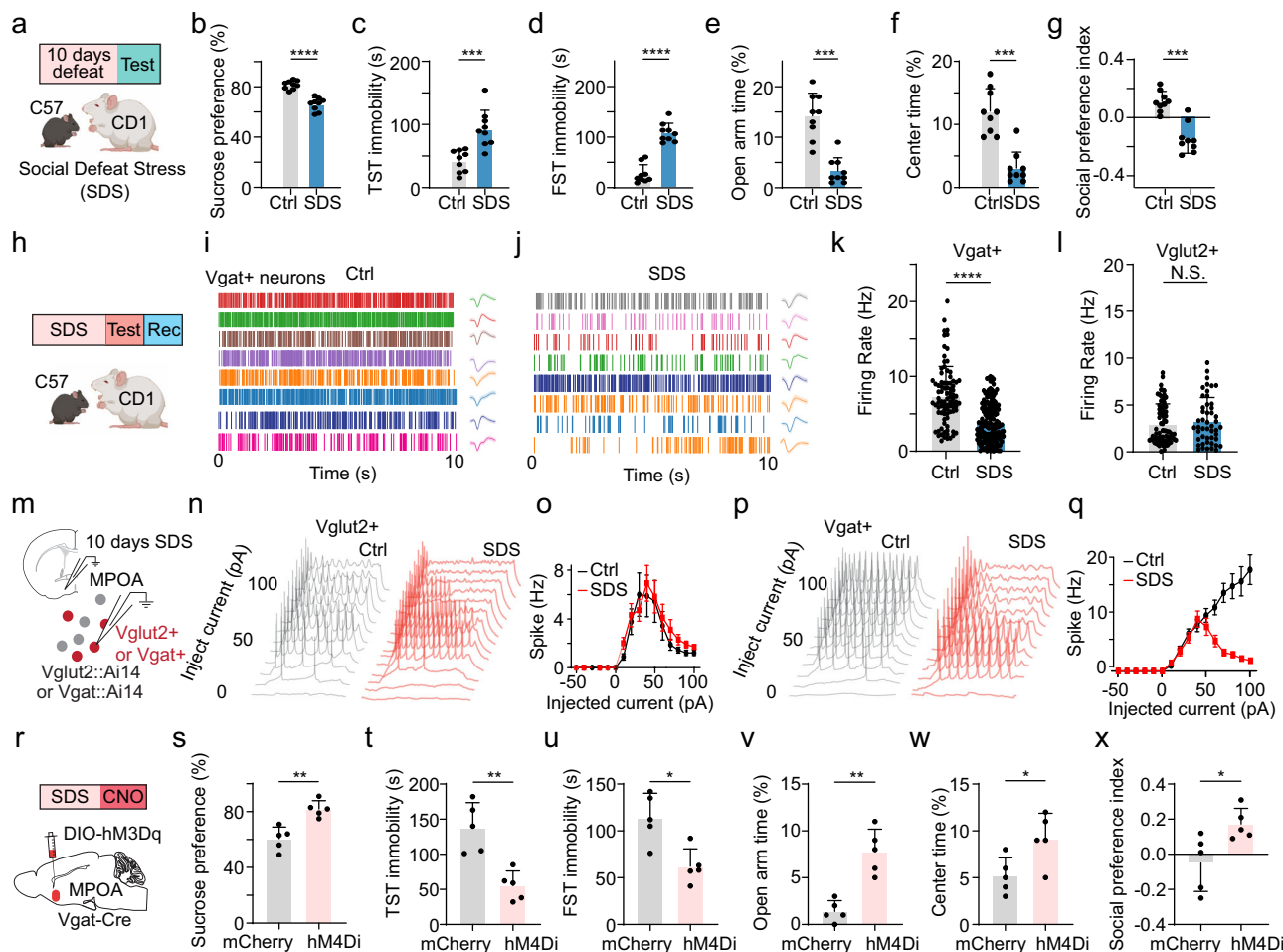


Fig. 6 | Reduced MPOA GABAergic activity following chronic social defeat stress.

a Schematic chronic social defeat stress. **b** Percentage sucrose water consumption. **c** Immobility time in TST. **d** Immobility time in FST. **e** Percentage time spent in opened arms of EPM. **f** Percentage time spent in the center in OFT. **g** Social preference index. Statistics, *** $p < 0.0001$ (**b**), *** $p = 0.0002$ (**c**), *** $p < 0.0001$ (**d**), *** $p = 0.0001$ (**e**), *** $p = 0.0002$ (**f**), *** $p = 0.0002$ (**g**), two-tailed Mann–Whitney test, $n = 9$ mice in each group. Data are presented as mean \pm s.d. **h** Schematic optrode recording in MPOA of SDS animals. **i, j** Raster plots of spontaneous spikes of eight ChR2-tagged Vgat+ neurons in control (**i**) and CRS (**j**) animals. Insets are superimposed spike waveforms for each unit. **k, l** Mean spontaneous spike rates of all the recorded Vgat+ (**k**) and Vglut2+ (**l**) neurons in control and CRS groups (**k**, $n = 87$ and 75 cells, respectively, from three animals in each group, *** $p < 0.0001$, two-tailed unpaired *t*-test; **l**, $n = 80$ and 48 cells, respectively, from three animals in each group, $p = 0.4268$, unpaired *t*-test). **m** Whole-cell recording from Vgat+ or Vglut2+

neurons after SDS treatment. **n** Example membrane potential responses to step-current injections in a control (gray) and SDS (red) Vglut2+ neuron. **o** Average input–output function of Vglut2+ neurons in control (gray) and SDS group ($n = 7$ and 7 cells, respectively, from three animals in each group). **p, q** Excitability of Vgat+ neurons in the control (gray) and SDS (red) group ($n = 9$ and 8 cells, respectively, from three animals in each group). **r** Schematic chemogenetic activation of Vgat+ neurons. **s** Percentage sucrose water consumption in mCherry- and hM4Di-expressing animals. **t** Immobility time in TST. **u** Immobility time in FST. **v** Percentage time spent in open arms of EPM. **w** Percentage time spent in the center in OFT. **x** Social preference index. Statistics, ** $p = 0.0079$ (**s**), *** $p = 0.0079$ (**t**), * $p = 0.0159$ (**u**), ** $p = 0.0079$ (**v**), * $p = 0.0476$ (**w**), * $p = 0.0317$ (**x**), two-tailed unpaired Mann–Whitney test, $n = 5$ mice for each group. Error bars represent s.e.m. in (**o**, **q**) and s.d. in the rest of the panels. For exact *p* values, see Source Data. (**a** and **h**) were created with BioRender.com.

while that from the Vgat+ to Vglut2+ neurons was prominent (Supplementary Fig. 9b, d–f). The latter is consistent with our previous finding¹³. These results suggest that activation of the Vglut2+ population would have limited impact on the Vgat+ population, while suppression of the Vgat+ population has the potential to lead to increased activity of the Vglut2+ population, which could then further increase the E/I ratio.

Discussion

Changes in excitatory and inhibitory activities and thus the E/I balance have long been postulated as a critical component in the pathology of MDD. However, the exact neuronal changes at circuit levels remain largely unclear. In the present study, we focused on the role of MPOA and its neuronal types in the neurobiology of depressive-like states, specifically under the context of chronic stress. We investigated how distinct forms of chronic stress uniquely modulate glutamatergic vs.

GABAergic neuronal activity and established a causal relationship between the activity changes and behavioral manifestations through cell-type-specific manipulations. Moreover, we investigated the PVH projection to the MPOA, which was found to primarily contribute to the induction but not expression phase, underscoring distinct functional roles of different hypothalamic structures in depressive-like behaviors. Furthermore, we investigated the functional roles of MPOA glutamatergic projections to the VTA and vIPAG regions and found that they orchestrate divergent depressive-like symptoms. Our findings highlight the potential centrality of MPOA within depression-related networks. Notably, the balance between excitatory and inhibitory outputs of MPOA to downstream midbrain structures emerges as a crucial determinant in both the manifestation and persistence of depressive-like behaviors.

In depression, alterations in excitation and inhibition can occur across multiple levels, including changes in neurotransmitter

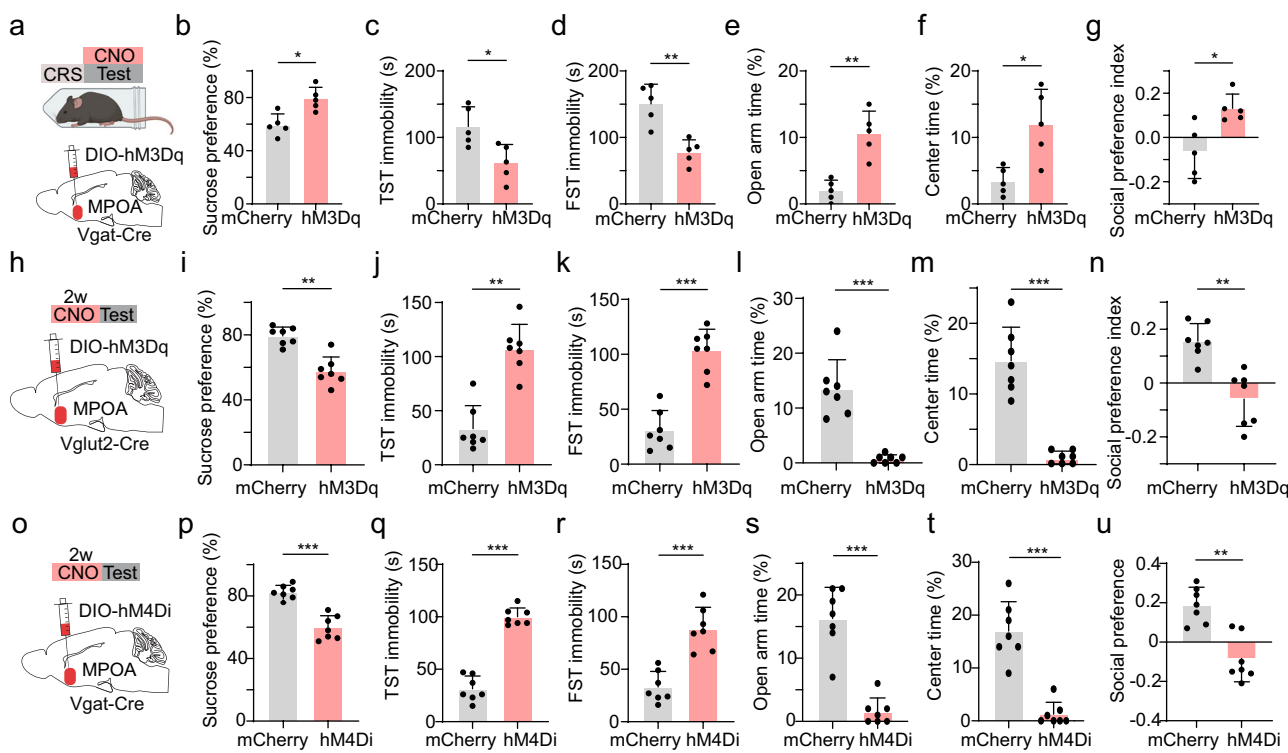


Fig. 7 | The MPOA E-I balance regulates depressive-like behaviors. **a** Schematic of viral injection and chemogenetic activation of MPOA GABAergic neurons in CRS animals. **b** Percentage sucrose water consumption in SPT with CNO injection in mCherry- and hM3Dq-expressing mice. **d** Immobility time in FST. **e** Percentage time spent in open arms of EPM. **f** Percentage time spent in the center in OFT. **g** Social preference index. Statistics, $p = 0.0159$ (**b**), $p = 0.0238$ (**c**), $**p = 0.0079$ (**d**), $*p = 0.0079$ (**e**), $*p = 0.0238$ (**f**), $*p = 0.0238$ (**g**), two-tailed Mann-Whitney test, $n = 5$ mice in each group. **h** Schematic of viral injection and chronic chemogenetic activation of MPOA glutamatergic neurons for 2 weeks. **i-n** Similar to (**b-g**) but for

chronic activation of glutamatergic neurons. $**p = 0.0012$ (**i**), $**p = 0.0012$ (**j**), $**p = 0.0006$ (**k**), $***p = 0.0006$ (**l**), $***p = 0.0006$ (**m**), $**p = 0.0012$ (**n**), two-tailed Mann-Whitney test, $n = 7$ mice in each group. **o** Schematic of viral injection and chronic chemogenetic suppression of MPOA GABAergic neurons. **p-u** Similar to (**i-n**) but for chronic suppression of GABAergic neurons. $***p = 0.0006$ (**p**), $***p = 0.0006$ (**q**), $***p = 0.0006$ (**r**), $***p = 0.0006$ (**s**), $***p = 0.0006$ (**t**), $**p = 0.0017$ (**u**), two-tailed Mann-Whitney test, $n = 7$ mice in each group. All error bars represent s.d. For exact p values, see Source Data. (**a**) was created with BioRender.com.

concentration^{11,31,32}, synaptic strength³³, cell number³⁴, and neuronal firing activity^{20,35}. Due to technical difficulties, specific brain regions exhibiting these pathological changes and playing a key role in mediating depressive states remain inconclusive³¹. For example, neuronal activity has been reported downregulated in the prefrontal cortex and optogenetic activation in this area suggests antidepressant effects³⁵. However, clinical trials targeting the prefrontal cortex using transcranial magnetic stimulation have yielded relatively low response rates in patients with MDD³⁶. Thus, other brain structures need to be further explored.

MPOA GABAergic neurons expressing estrogen receptors have been shown to play a key role in mediating depressive-like behaviors induced by ovarian hormone withdrawal¹⁹. However, it remains unclear whether the GABAergic population in the MPOA is specifically linked to depression associated with hormonal fluctuations, or if it can generally modulate depressive-like states arising from diverse etiological factors. In this study, in mice of both sexes exposed to chronic restraint stress, we found increased glutamatergic activity in the MPOA. This result is in fact consistent with our previous finding that MPOA glutamatergic neurons acutely respond to various stressors¹³ and suggests that chronic repeated activation has induced plastic changes in these neurons, resulting in their persistent hyperactivity. On the other hand, for the chronic social defeat paradigm, we observed decreased GABAergic activity in the MPOA, similar to the hormone withdrawal model¹⁸. Thus, across the three different depression models, there is a consistent net effect of an increased E-I ratio within the MPOA network, either by increasing excitatory or by decreasing inhibitory activity, suggesting that the increased E-I ratio is a key factor underlying

depressive-like states. Consistent with this idea, normalizing the E-I ratio through manipulating either excitatory or inhibitory activity can mitigate depressive-like behaviors, regardless of the type of stress exposed to. Furthermore, artificially disrupting the E-I balance in naïve mice can directly result in the manifestation of depressive-like behaviors while preventing changes in the MPOA E/I ratio during stress exposure preclude the development of depressive-like states. Based on all these results, we propose that the E-I balance in MPOA circuits is a critical factor in controlling depressive-like behaviors (Fig. 8), potentially through a regulatory effect on its downstream targets, in particular VTA and vIPAG (see below).

The E-I imbalance in MPOA is manifested by distinct changes in glutamatergic and GABAergic populations following chronic restraint and social defeat stress, respectively. The restraint stress specifically leads to enhanced glutamatergic activity, which is attributed to a combination of cellular- and network-level changes, including elevated intrinsic membrane excitability, increased excitatory synaptic input, enhanced basal-level spiking and emergence of burst-firing cells. By contrast, following chronic social stress, it is the GABAergic population that exhibits plasticity as reflected in the reduced intrinsic membrane excitability and baseline firing, with the glutamatergic population unaffected. These results indicate that the MPOA neuronal types have different susceptibility to different stressors. Cell-type dependent vulnerability has also been observed in other brain regions³⁷. For example, a study of depression using single-nucleus RNA sequencing suggests that excitatory neurons of the prefrontal cortex exhibit more pronounced gene expressional changes compared to inhibitory neurons³⁸. In the nucleus accumbens, D1- but not D2-expressing cells

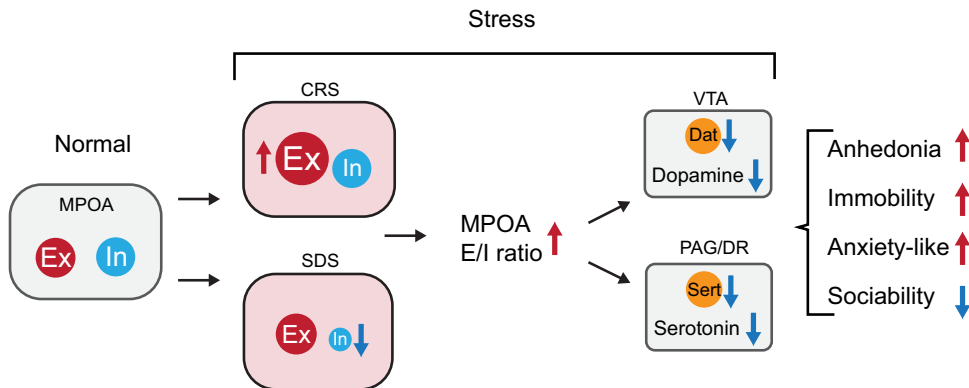


Fig. 8 | A working model for stress-induced changes in MPOA E-I balance. Under chronic restraint stress, there is an increase in excitation, while under social defeat stress, there is a decrease in inhibition. In both scenarios, there is an overall increase

in the excitation-inhibition ratio. This E-I imbalance is correlated with the induction and expression of depressive-like behaviors and decreased dopaminergic and serotonergic activities in downstream targets of MPOA.

exhibit reduced neurotrophin-2 expression in depression³⁹. In normal conditions, expression of membrane receptors in MPOA is largely distinct between excitatory and inhibitory populations, e.g., estrogen receptors are primarily expressed in its GABAergic population¹². Moreover, functional connectivity of the glutamatergic and GABAergic populations could be different. As one major source of excitatory input to MPOA, PVH has been shown to be more sensitive to restraint than social defeat stress⁴⁰. The excitatory PVH projection primarily targets the excitatory rather than the inhibitory population in MPOA (Fig. 4h, i) and is critical for the induction of depressive-like states under chronic restraint stress. These differences could lead to cell-type-dependent changes that result in E-I imbalance in MPOA following stress exposures.

Monoamine deficiency, especially regarding dopamine and serotonin, has long been thought to be involved in the pathology of MDD⁴¹. Both glutamatergic and GABAergic MPOA neurons project to VTA and PAG^{13,19}, two midbrain regions highly relevant to monoaminergic activity. The MPOA GABAergic population has been shown to promote the activity of midbrain dopaminergic and serotonergic neurons^{16,19,42}. In this study, we found that the activity of MPOA glutamatergic neurons suppresses midbrain dopaminergic and serotonergic neurons, thus functionally opposing the GABAergic population. With respect to depressive-like behaviors, the glutamatergic and GABAergic MPOA projections to the same target mediate the same set of behavioral phenotypes^{13,19} but in opposite directions: the one to VTA mediates anhedonia and the one to vPAG mediates immobility, while both contribute to social withdrawal. Thus, through parallel but competing excitatory and inhibitory projection pathways toward common targets, the MPOA outputs could exert a bidirectional control of the midbrain monoaminergic systems. The E-I balance of the MPOA output is thus a critical determinant of its modulatory effects on the monoaminergic systems. Such bidirectional control may allow a broader dynamic range and a finer scale to be achieved for the modulation, as compared to a unidirectional system.

We should acknowledge that our optogenetic terminal silencing experiments have certain limitations, with a potential for incomplete silencing at presynaptic terminals. Nevertheless, NpHR3.0 used in this study has been shown to be able to achieve more reliable terminal inhibition compared to ArchT^{26,27,43}. In addition, the use of NpHR3.0 for silencing MPOA long-range projections to VTA and PAG^{44,45} has generated behavioral effects opposite to the terminal activation with ChR2, which further supports the effectiveness of NpHR3.0 for terminal silencing.

Patients with MDD frequently present with a combination of symptoms such as social withdrawal⁴⁶, negative parenting style⁴⁷, anxiety⁴⁸, sexual dysfunction⁴⁹ and sleep deficits⁵⁰. Compared to other

structures in the widely distributed depression-related brain network, including VTA^{51,52}, medial prefrontal cortex^{35,53}, hippocampus⁵⁴, lateral habenula^{20,55,56}, dorsal raphe^{53,57,58}, amygdala⁵⁹, bed nucleus of the stria terminalis (BNST)⁶⁰, and ventral pallidum (VP)⁶¹, MPOA could serve as a unique therapeutic target when considering developing treatments. This is due to its diverse functional roles in regulating social reward perception¹⁶, sexual motivation⁶², parenting behavior^{14,15}, sleep^{20,63} and anxiety coping¹³. We speculate that rebalancing the E-I of MPOA circuits in the treatment of depression could offer numerous benefits by alleviating various symptoms. Both preclinical and clinical evidence support the notion that manipulating E-I balance in the brain by using ketamine or brexanolone can have fast antidepressant effects^{9,10}. Our current results have raised a possibility that these antidepressant effects may be achieved partially through rectifying the E-I imbalance in MPOA-midbrain circuits, which awaits to be tested in the future.

Our study raises a series of mechanistic-level questions. First, we found that the PVH→MPOA circuit is required for the induction of depressive-like states under restraint stress, suggesting that this pathway could be a potential target for preventing depression. How does this pathway drive plasticity in MPOA neurons? Is the process dependent on glutamatergic transmission or some neuropeptide release from PVH axons since PVH expresses a rich repertoire of peptides⁶⁴? Given that CRH-expressing PVH neurons in the hypothalamic-pituitary-adrenal (HPA) axis are well-documented to respond to acute and chronic stress⁶⁵, it is plausible that CRH-expressing PVH neurons may play a role in the induction phase. Although our retrograde tracing data revealed that MPOA-projecting PVH neurons mostly do not express CRH (Fig. 4f), it remains possible that CRH might impact MPOA circuits through endocrine mechanisms or some other peptides are involved, which awaits to be investigated.

Second, the increased sEPSCs in the CRS model are suggestive of enhanced glutamatergic transmission of the PVH-MPOA pathway, e.g., through an LTP-like synaptic plasticity mechanism. What is the dynamics of this plasticity, and can blocking it prevent the development of depressive-like states? On the other hand, the potential plasticity of the PVH-MPOA (as well as LHA-MPOA) pathway is dispensable for the expression of depressive-like behaviors (Fig. 4q-w), and no obvious changes in synaptic transmission have been observed in the SDS model (Supplementary Fig. 6a-h), suggesting that changes in intrinsic membrane excitability are probably the key factor underlying the manifestation of depressive-like states. If so, what membrane conductances have been altered to lead to enhanced excitability and increased burst firing in the glutamatergic population?

Third, although we have simply treated MPOA neurons as two functionally opposing cell types (excitatory vs. inhibitory), previous studies have revealed diverse molecularly determined cell types within

each of these functional groups and across the groups¹². It is possible that some specific cell types make larger contributions to the development of depressive-like behaviors than others under a specific depression-induction condition. For example, our previous study has shown that estrogen receptor 1 (Esrl) neurons in MPOA play an important role in the induction of depressive-like states by ovarian hormone withdrawal¹⁹. Identifying specific molecularly defined cell types in the MPOA that underlie depressive-like behaviors may provide more mechanistic insights in future investigations.

In summary, our study has highlighted MPOA as a critical hub to regulate affective state in response to chronic stress. Our results indicate that shifting the neuronal E-I balance of MPOA circuits toward excitation chronically can induce depressive-like states in animals, suggesting a common mechanism for depression linked to various etiological factors. Therefore, targeting the MPOA E-I balance may be a compelling strategy for developing therapeutic treatments for depression.

Methods

Animals

Animals. Our study utilized mice from various strains, including the Vglut2-ires-Cre (Jackson stock No. 016963), Vgat-ires-Cre (Jackson stock No. 016962), Vglut2-flpO (Jackson Stock No. 030212), Ai14 (Cre-dependent tdTomato reporter line, Jackson stock No. 007914), Ai27 (Cre-dependent ChR2 reporter line, Jackson stock No. 012567), Dat-ires-Cre (Jackson stock No. 006660), Sert-ires-Cre (Jackson stock No. 014554), C57BL/6. All these strains were obtained from Jackson Laboratories.

Housing and conditions. Post-weaning, the mice were group-housed based on their sex, with either their Cre-expressing or wild-type littermates, until they underwent surgery or behavioral testing. Both female and male mice were used. The living conditions provided to the mice were consistent with a 12-h light cycle (lights off at 18:00). Housing temperature was 65–75 °F and humidity was 40–60%. The mice were given unlimited access to food and water, except during specified times for behavioral testing.

Ethical compliance. All the procedures conducted in this study adhered strictly to the Guide for the Care and Use of Laboratory Animals, as adopted by the NIH. The study received full approval from the Institutional Animal Care and Use Committee (IACUC) at the University of Southern California, ensuring that the animals' welfare was prioritized throughout the study.

Procedures

General procedure for viral injection. To begin with, the mice were anesthetized using 1.5–2% isoflurane. A minor incision was made on the skin where the craniotomy was planned, followed by removal of the muscles. A craniotomy window was created for each region. Adeno-associated viruses (AAVs), encoding for different proteins including ChR2, eNpHR3.0, hM4D(Gi), hM3D(Gq), GFP, EYFP, mCherry, GCaMP7s, and ChrimsonR, were introduced as per the experiment's purpose and the mouse strain. The virus was delivered using a beveled glass micropipette filled with the viral solution, attached to a micro-syringe pump. Depending on the needs of the experiment, pressure injection or iontophoresis was used for virus delivery. In case of pressure injection, a small amount of viral solution (50–80 nl) was injected at a steady rate (15–25 nl/min). For iontophoretic injection, a current of 3–5 μA (cycle of 7 s on, 7 s off) was applied for 3–5 min. After each injection, the pipette was left in place for an additional 5 min before being withdrawn. The skin was then sutured. Prior to the surgery, pain management drugs, slow-release buprenorphine and ketoprofen were subcutaneously injected. The mice were allowed a recovery period of at least 1 week before further procedures. After

each experiment, the harvested brain was sectioned and imaged to confirm viral expression.

Stereotaxic coordinates. The coordinates used for the injections were as follows: MPOA: AP +0.6 mm, ML +1.3 mm, DV –4.75 mm, with a 10° angle; vIPAG: AP –4.4, ML +1.5 mm, DV –2.2 mm; VTA: AP –3.18 mm, ML +1.2 mm, DV –4.0 mm, with a 10° angle.

Viral constructs. We used a variety of AAV vectors, including AAV2/1-pEF1a-DIO-hChR2-eYFP (1.82×10^{13} genome copies (GC) ml⁻¹, UPenn vector core), AAV1-CAG-FLEX-GFP-WPRE (2×10^{13} GC ml⁻¹, UPenn vector core, Addgene, 51502), AAVretro-Cre (1.5×10^{14} GC ml⁻¹, Vigenie), AAV1-CAG-FLEX-ArchT-GFP (4×10^{12} GC ml⁻¹, UNC vector core), pAAV-hSyn-DIO-hM3D(Gq)-mCherry (1.3×10^{13} GC ml⁻¹, Addgene, 44361), pAAV-hSyn-DIO-hM4D(Gi)-mCherry (3×10^{13} GC ml⁻¹, Addgene, 44362), pAAV-hSyn-DIO-mCherry (4.8×10^{13} GC ml⁻¹, Addgene, 50459), AAV1-Syn-FLEX-GCamp7s-WPRE-SV4 (Addgene, 100845), AAV1-DIO-FLPo-WPRE-hGhpA (1.53×10^{14} GC ml⁻¹, Addgene, 87306), AAV5-Syn-FLEX-rc[ChrimsonR-tdTomato] (8.5×10^{12} GC ml⁻¹, Addgene, 62723-AAV5).

Fiber and cannula implantation. For optogenetic manipulations, animals were anesthetized 2 weeks post viral injection with isoflurane, and optic cannulas were stereotactically implanted into the targeted region based on the purpose of experiments (bilateral MPOA, bilateral VTA, bilateral vIPAG). The GRIN lens was used for monitoring single neuronal calcium activities in MPOA (unilateral). The optic cannula was secured with dental cement. The mice were allowed to recover for at least 1 week before the behavior tests. After experiments, the brain was harvested, sectioned and imaged to confirm locations of viral expression and the implantation site. Animals showing significant leakage to surrounding regions were excluded from the analysis.

RNA in situ hybridization

Animals were first thoroughly anesthetized and then perfused with PBS and a 4% solution of Paraformaldehyde (PFA). The brains were subsequently dissected and left to fix overnight. Following fixation, the brains were dehydrated, and cryosections of 30-μm thickness were collected and mounted on Superfrost Plus slides. For RNAscope staining, we utilized the RNAscope Multiplex Fluorescent Detection Assay V2 kit (Advanced Cell Diagnostics, 323100), following the manufacturer's recommended protocol. Brain sections were hybridized using a mix of RNAscope probes for Cre (Advanced Cell Diagnostics, 312281), Vglut2 (Advanced Cell Diagnostics, 319171), and Vgat (Advanced Cell Diagnostics, 319191), all of which were designed and validated by Advanced Cell Diagnostics. The signals from these probes were then amplified and marked with fluorescent dyes. Imaging of the samples was conducted using confocal microscopy. The obtained images were then processed using ImageJ software for further analysis.

Optogenetic stimulation

Prior to behavioral testing, animals underwent a minimum of two habituation sessions lasting 10 min each, where they became accustomed to handling and patch cable tethering in their home cage. Optogenetic manipulation was conducted using an LED light source (470 nm, 570 nm, or 625 nm) which delivered approximately 5 mW of light through an optic cable. For photoactivation with ChR2, 470 nm light was pulsed at 10–20 Hz with a pulse duration of 5 ms. ChrimsonR-based photo-tagging used 625 nm light pulsed at 5, 10, and 15 Hz with a pulse duration of 5 ms. Photoinhibition utilized 570 nm light delivered in a pattern of 10 s on and 5 s off to minimize the habituation and rebound responses of the channel. The use of eNpHR in terminal silencing has been rigorously evaluated in previous studies. It has been found that NpHR can achieve reliable terminal inhibition^{26,27,43}. Furthermore, the use of NpHR for silencing MPOA long-range projections

to VTA and PAG^{44,45} has been tested, which generates opposite behavioral effects to terminal activation. These pieces of evidence support that the NpHR could be appropriate for terminal silencing in this study. Throughout these procedures, animals were able to move freely within the testing chambers or home cages. Customized Python code and Arduino microcontrollers were used to control light delivery for each behavioral assay.

Chemogenetics

For in vivo chemogenetic experiments, animals expressing hM4D(Gi) or hM3D(Gq) were given an intraperitoneal (i.p.) injection of clozapine-N-oxide (CNO) at a dosage of 1 mg/kg, 20 min before behavioral tests. To verify the efficiency and effects of CNO on neurons expressing hM4D(Gi) or hM3D(Gq), *in vitro* chemogenetic experiments were performed. Whole-cell patch clamp recording was used to examine membrane potential responses before and after the perfusion of CNO (10 µM).

Behavioral tests

Sucrose preference test (SPT). After 24 h of water deprivation, animals were given access to two bottles for 1 h: one containing 2% sucrose water and the other, pure water. If optogenetic manipulation was involved, it was administered throughout the testing period. The sucrose consumption ratio was then computed by dividing the volume of sucrose water consumed by the total volume of water consumed from both bottles.

Tail suspension test (TST). This involved suspending the mouse by its tail using tape, the other end of which was situated 40 cm off the ground. Over a 6-min period, the mouse's behavior was recorded. If optogenetic manipulation was involved, it was delivered immediately upon placing the mice in the testing chamber, lasting for 6 min. The duration of immobility was measured by scoring a video recording of the experiment, which was performed blindly and automatically after testing using customized scripts as detailed below.

Forced swimming test (FST). Animals were individually introduced into a cylinder filled with water (23–25 °C) to a depth that prevented them from touching the bottom with their tails or hind limbs. They swam for 6 min under regular light conditions. During the last 4 min of the test, any time spent immobile, which is defined as remaining afloat or motionless except for balance-keeping movements, was scored automatically. If optogenetic manipulation was involved, it was delivered right after placing the mice in the water and lasted for 6 min.

Elevated plus maze test (EPM). A cross-shaped maze with two closed and two open arms, elevated 30 cm above ground, was used. Mice were placed at the center of the maze, and their movements were recorded for 10 min. If optogenetic manipulation was involved, it was given immediately upon placing the mice in the apparatus and lasted for 10 min. The optic cable was hoisted by a helium balloon to minimize its impact on locomotion. The time spent on the open arm was scored automatically by a customized code.

Open field test (OFT). The test was conducted in a white box (60 × 60 × 30 cm), divided into a central area (30 × 30 cm) and a peripheral field. Mice were placed in the periphery, and their movements were recorded over 20 min. The time spent in the center was automatically scored by customized code.

Parental behavior test. The test was conducted in the home cage after a 30-min habituation period. A pup younger than P5 was placed in a corner of the home cage. Each test was recorded, and the grooming time was scored automatically.

Social preference test. This test used a three-chamber box. Two clean, empty wire cups were inverted and placed on opposite sides of the box. After a 20-min habituation period, the test mouse was introduced to the central chamber. A juvenile same sex mouse (4–5 weeks old) unfamiliar to the test mouse was placed in one of the cups. The social preference index was then calculated by dividing the difference in time spent in the social versus the non-social chamber by the total time spent in both chambers. Time spent in each chamber was automatically scored by customized code.

In vivo optrode recording and spike sorting

Specific neuronal types were genetically tagged through the crossing of Cre line with Ai27, which is a Cre-dependent ChR2 reporter line, or through injection of Cre-dependent ChR2 or ChrimsonR in a Cre mouse line, as detailed in each experiment. We conducted multi-channel recordings utilizing a 64-channel silicone probe (A1x64-Poly2-6mm-23s-160-OA64LP, with 64 contacts separated by 23 µm, a fiber of 105 µm, N.A. 0.22, and the termination of the fiber being 50 µm above the top recording site, Neuronexus Technologies). The probe was connected to an LED light source (480 or 625 nm depending on the experiment, from Thorlabs) via an optic fiber. Signals were recorded using the OpenEphys system and filtered through a bandpass filter ranging from 0.3 to 30 kHz. We grouped the nearest four channels of the probe as tetrodes and executed semi-automated spike sorting with the Offline Sorter (V4, Plexon Inc.). We used negative 3-fold standard deviations from the mean peak heights histogram as the waveform detection threshold. Template matching clustering was carried out based on the spike waveform on each tetrode channel. Clusters that showed isolation distance <20 and L-Ratio >0.1 were disregarded. We classified spike clusters as single units only if the waveform Signal-to-Noise Ratio (SNR) was greater than 4 (12 dB) and if the inter-spike intervals surpassed 1.2 ms for more than 99.5% of the spikes.

To identify ChR2+ neurons, we delivered LED pulse trains (5-ms pulse duration, 100-ms total duration, controlled via an Arduino microcontroller) intermittently at 5 or 10 Hz. We analyzed the onset latency relative to each light pulse to determine whether these units were driven directly by ChR2 or indirectly by synaptic connections. In this study, only spikes with latency less than 4 ms were considered as being directly stimulated. We analyzed the waveform similarity between LED-evoked and spontaneously generated spikes, using a correlation coefficient greater than 0.9 as the criterion for determining if they originated from the same unit.

Image acquisition

To check the expression of eYFP, GFP or mCherry, or electrode tracks (coated with Dil), the animals were deeply anesthetized using isoflurane and transcardially perfused with phosphate-buffered saline (PBS) and paraformaldehyde (4% in PBS). Coronal brain sections (150 µm) were made with a vibratome (Leica Microsystems) and stained with Nissl reagent (Deep red, Invitrogen) for 2 h at room temperature. Each slice was imaged under a confocal microscope (Olympus).

Behavioral data analysis

Markerless pose estimation were based on Faster-RCNN and HRnet using mmopenlab framework, annotations were semi-automatically performed, and training was initiated using customized configuration file (written by Guangwei Zhang, in Python 3.7). For the forced swimming test and tail suspension test, kicks frequency was extracted and sorted, based on which the time of immobility can be calculated. The behavior analysis was blindly performed in a batch process and cross-compared with human classification to verify the accuracy to categorize the mobility and immobility time. Moreover, extracted optic

flow has also been used to assist the differentiation of mobility and immobility.

Miniscope recording

We employed the UCLA miniscope system (Miniscope V4, Open-Ephys), which allows for *in vivo* calcium imaging in freely moving animals. Animals were first anesthetized as described above. A small cranial window was drilled above the MPOA, and the GRIN lens was implanted (AP +0.6 mm, ML 0.5 mm, DV 4.2–4.6 mm). Post-operative care included administration of analgesics to prevent pain. Animals were allowed to recover for at least 7 days before imaging. Viral vectors encoding GCaMP7s were injected into MPOA (AP +0.6 mm, ML 0.5 mm, DV 4.2–4.6 mm, 80 nl) 2–3 weeks prior to imaging to allow for sufficient expression. Animals were allowed to freely move in an open field arena while being tethered to the miniscope recording system. Imaging was conducted at 30 Hz with a resolution of 640 × 480 pixels. Each recording session lasted for 15 min. The raw videos were first corrected for motion artifacts using the NoRMCorre algorithm⁶⁶. Background fluorescence was then subtracted using a rolling ball algorithm. To extract individual neuron calcium activity, regions of interest (ROIs) corresponding to individual neurons were identified using the CNMF-E algorithm⁶⁷, which decomposes the video into spatial and temporal components. For each identified ROI, the temporal fluorescence trace was extracted. This trace represents the raw calcium signal of the neuron. $\Delta F/F_0$ was calculated by taking the difference between the current fluorescence value (F) and the baseline fluorescence (F_0), and then dividing by F_0 . The baseline fluorescence (F_0) was determined using a moving average. Neurons across days were pair-wise matched using CellReg⁶⁸, based on the similarity matrix of locations and shapes.

Slice recording

Animals were decapitated following isoflurane anesthesia, and the brain was rapidly removed and immersed in an ice-cold dissection buffer (composition: 60 mM NaCl, 3 mM KCl, 1.25 mM NaH_2PO_4 , 25 mM NaHCO_3 , 115 mM sucrose, 10 mM glucose, 7 mM MgCl_2 , 0.5 mM CaCl_2 ; saturated with 95% O_2 and 5% CO_2 ; pH = 7.4). Coronal slices at 350 μm thickness were sectioned by a vibrating microtome (Leica VT1000S) and recovered for 30 min in a submersion chamber filled with warmed (35 °C) ACSF (composition: 119 mM NaCl, 26.2 mM NaHCO_3 , 11 mM glucose, 2.5 mM KCl, 2 mM CaCl_2 , 2 mM MgCl_2 , and 1.2 NaH_2PO_4 , 2 mM Sodium Pyruvate, 0.5 mM VC). MPOA neurons labeled by tdTomato fluorescence were visualized under a fluorescence microscope (Olympus BX51 WI). Patch pipettes (~4–5 MΩ resistance) filled with a cesium-based internal solution (composition: 125 mM cesium gluconate, 5 mM TEA-Cl, 2 mM NaCl, 2 mM CsCl, 10 mM HEPES, 10 mM EGTA, 4 mM ATP, 0.3 mM GTP, and 10 mM phosphocreatine; pH = 7.25; 290 mOsm) were used for targeted whole-cell recordings. Signals were recorded with an Axopatch 700B amplifier (Molecular Devices) under current clamp to examine spontaneous spiking, and then –50 pA to +100 pA square currents (at 10 pA step) were injected to test membrane potential responses. Under voltage clamp mode, holding voltage of –70 mV or 0 mV was applied for recording excitatory or inhibitory synaptic currents, respectively. Signals were filtered at 2 kHz and sampled at 10 kHz. To confirm the connectivity between PVH axons and MPOA glutamatergic neurons, tetrodotoxin (TTX, 1 μM) and 4-aminopyridine (4-AP, 1 mM) were added to the external solution for recording monosynaptic responses to blue light stimulation (5 ms pulse, 3 mW power, 10–30 trials). At the end of experiment, CNQX (20 μM , Sigma-Aldrich) was added to the external solution to confirm glutamatergic currents.

For testing the efficacies of ChR2, ArchT and hM4D(Gi), hM3D(Gq), brain slices were prepared similarly, and whole-cell current clamp recordings were made from neurons expressing ChR2, ArchT, hM4D(Gi) or hM3D(Gq). A train of blue light pulses at different

frequencies (1–20 Hz, 5-ms pulse duration) was applied to measure spike responses of ChR2-expressing neurons. Green light stimulation (10-s duration) was applied to measure hyperpolarization in ArchT-expressing neurons. For neurons expressing hM4D(Gi) or hM3D(Gq), spontaneous spikes were recorded before and after perfusion of CNO (10 μM) and after washing out CNO.

Statistics

Prior power analysis was not used to determine sample sizes. Sample sizes were selected based on previous experience from related research or literature^{15–17,69}. Animals were randomly assigned to control and treatment groups. For animals with multiple assays, the sequence of assays was randomized. Investigators were not blinded to group allocation or data collection, but the analyses of behavioral data were performed blind to the conditions of experiments, as data obtained under different conditions were pooled together for an automatic batch analysis with computer software. Prism version 8 software (GraphPad) and R were used for statistical analysis. The Kolmogorov–Smirnov test was used to test for normality. The Mann–Whitney test was used for non-normally distributed data. One-way ANOVA and two-way ANOVA and post hoc Tukey's multiple comparisons were used to test the significance between samples. For two-group comparison of normal data, significance was determined by *t*-test. Paired *t*-tests were used to compare data from the same animal. In this study, animals with failed viral expression or fiber implantation were excluded from the analysis.

Statistics and sampling determination

R (<https://www.r-project.org/>) was used for the statistical analysis.

Reporting summary

Further information on research design is available in the Nature Portfolio Reporting Summary linked to this article.

Data availability

Source data are provided with this paper. Other data that support the findings of this study are available from the corresponding author upon request.

Code availability

The code used for animal detection is available on <https://github.com/GuangWei-Zhang/Mouse-behavioral-annotation> (<https://doi.org/10.5281/zenodo.13381825>). Other code that supports the findings of this study is available from the corresponding author upon request.

References

1. Nelson, S. B. & Valakh, V. Excitatory/inhibitory balance and circuit homeostasis in autism spectrum disorders. *Neuron* **87**, 684–698 (2015).
2. Sohal, V. S. & Rubenstein, J. L. R. Excitation-inhibition balance as a framework for investigating mechanisms in neuropsychiatric disorders. *Mol. Psychiatry* **24**, 1248–1257 (2019).
3. Rubenstein, J. L. R. & Merzenich, M. M. Model of autism: increased ratio of excitation/inhibition in key neural systems. *Genes Brain Behav.* **2**, 255–267 (2003).
4. Yizhar, O. et al. Neocortical excitation/inhibition balance in information processing and social dysfunction. *Nature* **477**, 171–178 (2011).
5. Lisman, J. Excitation, inhibition, local oscillations, or large-scale loops: what causes the symptoms of schizophrenia? *Curr. Opin. Neurobiol.* **22**, 537–544 (2012).
6. Hu, Y.-T., Tan, Z.-L., Hirjak, D. & Northoff, G. Brain-wide changes in excitation-inhibition balance of major depressive disorder: a systematic review of topographic patterns of GABA- and glutamatergic alterations. *Mol. Psychiatry* **28**, 3257–3266 (2023).

7. Krishnan, V. & Nestler, E. J. The molecular neurobiology of depression. *Nature* **455**, 894–902 (2008).
8. Kanner, A. M. & Balabanov, A. Depression and epilepsy: how closely related are they? *Neurology* **58**, S27–S39 (2002).
9. Serafini, G. et al. The role of ketamine in treatment-resistant depression: a systematic review. *Curr. Neuropharmacol.* **12**, 444–461 (2014).
10. Meltzer-Brody, S. et al. Brexanolone injection in post-partum depression: two multicentre, double-blind, randomised, placebo-controlled, phase 3 trials. *Lancet* **392**, 1058–1070 (2018).
11. Luscher, B., Shen, Q. & Sahir, N. The GABAergic deficit hypothesis of major depressive disorder. *Mol. Psychiatry* **16**, 383–406 (2011).
12. Moffitt, J. R. et al. Molecular, spatial, and functional single-cell profiling of the hypothalamic preoptic region. *Science* **362**, eaau5324 (2018).
13. Zhang, G.-W. et al. Medial preoptic area antagonistically mediates stress-induced anxiety and parental behavior. *Nat. Neurosci.* **24**, 516–528 (2021).
14. Fang, Y.-Y., Yamaguchi, T., Song, S. C., Tritsch, N. X. & Lin, D. A hypothalamic midbrain pathway essential for driving maternal behaviors. *Neuron* **98**, 192–207.e10 (2018).
15. Wu, Z., Autry, A. E., Bergan, J. F., Watabe-Uchida, M. & Dulac, C. G. Galanin neurons in the medial preoptic area govern parental behaviour. *Nature* **509**, 325–330 (2014).
16. McHenry, J. A. et al. Hormonal gain control of a medial preoptic area social reward circuit. *Nat. Neurosci.* **20**, 449–458 (2017).
17. Hu, R. K. et al. An amygdala-to-hypothalamus circuit for social reward. *Nat. Neurosci.* **24**, 831–842 (2021).
18. Santollo, J., Torregrossa, A.-M. & Eckel, L. A. Estradiol acts in the medial preoptic area, arcuate nucleus, and dorsal raphe nucleus to reduce food intake in ovariectomized rats. *Horm. Behav.* **60**, 86–93 (2011).
19. Tao, C. et al. The medial preoptic area mediates depressive-like behaviors induced by ovarian hormone withdrawal through distinct GABAergic projections. *Nat. Neurosci.* **26**, 1529–1540 (2023).
20. Yang, Y. et al. Ketamine blocks bursting in the lateral habenula to rapidly relieve depression. *Nature* **554**, 317–322 (2018).
21. Xiao, C. et al. Glutamatergic and GABAergic neurons in pontine central gray mediate opposing valence-specific behaviors through a global network. *Neuron* **111**, 1486–1503.e7 (2023).
22. Shen, L. et al. A bottom-up reward pathway mediated by somatostatin neurons in the medial septum complex underlying appetitive learning. *Nat. Commun.* **13**, 1194 (2022).
23. Smith, J. et al. Regulation of stress-induced sleep fragmentation by preoptic glutamatergic neurons. *Curr. Biol.* **34**, 12–23.e5 (2023).
24. Dimén, D. et al. Sex-specific parenting and depression evoked by preoptic inhibitory neurons. *iScience* **24**, 103090 (2021).
25. Li, Z. et al. Corticostratial control of defense behavior in mice induced by auditory looming cues. *Nat. Commun.* **12**, 1040 (2021).
26. Emiliani, V. et al. Optogenetics for light control of biological systems. *Nat. Rev. Methods Prim.* **2**, 1–25 (2022).
27. Kaneda, K. et al. Selective optical control of synaptic transmission in the subcortical visual pathway by activation of viral vector-expressed halorhodopsin. *PLoS ONE* **6**, e18452 (2011).
28. Pollak Dorocic, I. et al. A whole-brain atlas of inputs to serotonergic neurons of the dorsal and median raphe nuclei. *Neuron* **83**, 663–678 (2014).
29. Becker, C. et al. Repeated social defeat-induced depression-like behavioral and biological alterations in rats: involvement of cholecystokinin. *Mol. Psychiatry* **13**, 1079–1092 (2008).
30. Berton, O. et al. Essential role of BDNF in the mesolimbic dopamine pathway in social defeat stress. *Science* **311**, 864–868 (2006).
31. Sanacora, G., Zarate, C. A., Krystal, J. H. & Manji, H. K. Targeting the glutamatergic system to develop novel, improved therapeutics for mood disorders. *Nat. Rev. Drug Discov.* **7**, 426–437 (2008).
32. Hashimoto, K., Sawa, A. & Iyo, M. Increased levels of glutamate in brains from patients with mood disorders. *Biol. Psychiatry* **62**, 1310–1316 (2007).
33. Durman, R. S., Aghajanian, G. K., Sanacora, G. & Krystal, J. H. Synaptic plasticity and depression: new insights from stress and rapid-acting antidepressants. *Nat. Med.* **22**, 238–249 (2016).
34. Chen, F. et al. Hippocampal volume and cell number in depression, schizophrenia, and suicide subjects. *Brain Res.* **1727**, 146546 (2020).
35. Covington, H. E. et al. Antidepressant effect of optogenetic stimulation of the medial prefrontal cortex. *J. Neurosci.* **30**, 16082–16090 (2010).
36. Holtzheimer, P. E. & Mayberg, H. S. Deep brain stimulation for treatment-resistant depression. *AJP* **167**, 1437–1444 (2010).
37. Northoff, G. & Sibille, E. Why are cortical GABA neurons relevant to internal focus in depression? A cross-level model linking cellular, biochemical and neural network findings. *Mol. Psychiatry* **19**, 966–977 (2014).
38. Nagy, C. et al. Single-nucleus transcriptomics of the prefrontal cortex in major depressive disorder implicates oligodendrocyte precursor cells and excitatory neurons. *Nat. Neurosci.* **23**, 771–781 (2020).
39. Heshmati, M. et al. Cell-type-specific role for nucleus accumbens neuregulin-2 in depression and stress susceptibility. *Proc. Natl Acad. Sci. USA* **115**, 1111–1116 (2018).
40. Motta, S. C. & Canteras, N. S. Restraint stress and social defeat: what they have in common. *Physiol. Behav.* **146**, 105–110 (2015).
41. Hamon, M. & Blier, P. Monoamine neurocircuitry in depression and strategies for new treatments. *Prog. Neuropsychopharmacol. Biol. Psychiatry* **45**, 54–63 (2013).
42. Bayless, D. W. et al. A neural circuit for male sexual behavior and reward. *Cell* **186**, 3862–3881.e28 (2023).
43. Li, Z. et al. Enhancement and contextual modulation of visuospatial processing by thalamocollicular projections from ventral lateral geniculate nucleus. *Nat. Commun.* **14**, 7278 (2023).
44. Kohl, J. et al. Functional circuit architecture underlying parental behaviour. *Nature* **556**, 326–331 (2018).
45. Ryoo, J., Park, S. & Kim, D. An inhibitory medial preoptic circuit mediates innate exploration. *Front. Neurosci.* **15**, 716147 (2021).
46. Girard, J. M. et al. Nonverbal social withdrawal in depression: evidence from manual and automatic analyses. *Image Vis. Comput.* **32**, 641–647 (2014).
47. Lovejoy, M. C., Graczyk, P. A., O'Hare, E. & Neuman, G. Maternal depression and parenting behavior: a meta-analytic review. *Clin. Psychol. Rev.* **20**, 561–592 (2000).
48. Tiller, J. W. G. Depression and anxiety. *Med. J. Aust.* **199**, S28–S31 (2013).
49. Williams, K. & Reynolds, M. F. Sexual dysfunction in major depression. *CNS Spectr.* **11**, 19–23 (2006).
50. Wallace, D. D., Boynton, M. H. & Lytle, L. A. Multilevel analysis exploring the links between stress, depression, and sleep problems among two-year college students. *J. Am. Coll. Health* **65**, 187–196 (2017).
51. Tye, K. M. et al. Dopamine neurons modulate neural encoding and expression of depression-related behaviour. *Nature* **493**, 537–541 (2013).
52. Chaudhury, D. et al. Rapid regulation of depression-related behaviours by control of midbrain dopamine neurons. *Nature* **493**, 532–536 (2013).
53. Warden, M. R. et al. A prefrontal cortex-brainstem neuronal projection that controls response to behavioural challenge. *Nature* **492**, 428–432 (2012).
54. Ramirez, S. et al. Activating positive memory engrams suppresses depression-like behaviour. *Nature* **522**, 335–339 (2015).
55. Proulx, C. D. et al. A neural pathway controlling motivation to exert effort. *Proc. Natl Acad. Sci. USA* **115**, 5792–5797 (2018).

56. Matsumoto, M. & Hikosaka, O. Lateral habenula as a source of negative reward signals in dopamine neurons. *Nature* **447**, 1111–1115 (2007).
57. Challis, C., Beck, S. G. & Berton, O. Optogenetic modulation of descending prefrontocortical inputs to the dorsal raphe bidirectionally bias socioaffective choices after social defeat. *Front. Behav. Neurosci.* **8**, 43 (2014).
58. Ohmura, Y. et al. Different roles of distinct serotonergic pathways in anxiety-like behavior, antidepressant-like, and anti-impulsive effects. *Neuropharmacology* **167**, 107703 (2020).
59. Cai, Y.-Q., Wang, W., Paulucci-Holthausen, A. & Pan, Z. Z. Brain circuits mediating opposing effects on emotion and pain. *J. Neurosci.* **38**, 6340–6349 (2018).
60. Johnson, S. B. et al. A basal forebrain site coordinates the modulation of endocrine and behavioral stress responses via divergent neural pathways. *J. Neurosci.* **36**, 8687–8699 (2016).
61. Knowland, D. et al. Distinct ventral pallidal neural populations mediate separate symptoms of depression. *Cell* **170**, 284–297.e18 (2017).
62. Wei, Y.-C. et al. Medial preoptic area in mice is capable of mediating sexually dimorphic behaviors regardless of gender. *Nat. Commun.* **9**, 279–279 (2018).
63. Chung, S. et al. Identification of preoptic sleep neurons using retrograde labelling and gene profiling. *Nature* **545**, 477–481 (2017).
64. Berkhouit, J. B. et al. An integrated single-cell RNA-seq atlas of the mouse hypothalamic paraventricular nucleus links transcriptomic and functional types. *J. Neuroendocrinol.* **36**, e13367 (2024).
65. Holsboer, F. The corticosteroid receptor hypothesis of depression. *Neuropsychopharmacology* **23**, 477–501 (2000).
66. Pnevmatikakis, E. A. & Giovannucci, A. NoRMCorre: an online algorithm for piecewise rigid motion correction of calcium imaging data. *J. Neurosci. Methods* **291**, 83–94 (2017).
67. Zhou, P. et al. Efficient and accurate extraction of *in vivo* calcium signals from microendoscopic video data. *eLife* **7**, e28728 (2018).
68. Sheintuch, L. et al. Tracking the same neurons across multiple days in Ca^{2+} imaging data. *Cell Rep.* **21**, 1102–1115 (2017).
69. Mei, L., Yan, R., Yin, L., Sullivan, R. M. & Lin, D. Antagonistic circuits mediating infanticide and maternal care in female mice. *Nature* **618**, 1006–1016 (2023).

Acknowledgements

This work was supported by grants from the US National Institutes of Health (EY019049 and MH116990 to H.W.T.; DC008983, DC020887, NS132912 and MH116990 to L.I.Z.).

Author contributions

H.W.T. and L.I.Z. conceived the study and supervised the project. C.T. and G.W.Z. performed most of the experiments and data analysis. C.T. performed slice recordings and data analysis. W.S. helped with the miniscope recording. J.J.H. helped with the animal breeding and behavioral tests. H.W.T., C.T., G.W.Z. and L.I.Z. wrote the manuscript.

Competing interests

The authors declare no competing interests.

Additional information

Supplementary information The online version contains supplementary material available at <https://doi.org/10.1038/s41467-024-52727-2>.

Correspondence and requests for materials should be addressed to Li I. Zhang or Huizhong Whit Tao.

Peer review information *Nature Communications* thanks Haohong Li, Árpád Dobolyi and the other anonymous reviewers for their contribution to the peer review of this work. A peer review file is available.

Reprints and permissions information is available at <http://www.nature.com/reprints>

Publisher's note Springer Nature remains neutral with regard to jurisdictional claims in published maps and institutional affiliations.

Open Access This article is licensed under a Creative Commons Attribution-NonCommercial-NoDerivatives 4.0 International License, which permits any non-commercial use, sharing, distribution and reproduction in any medium or format, as long as you give appropriate credit to the original author(s) and the source, provide a link to the Creative Commons licence, and indicate if you modified the licensed material. You do not have permission under this licence to share adapted material derived from this article or parts of it. The images or other third party material in this article are included in the article's Creative Commons licence, unless indicated otherwise in a credit line to the material. If material is not included in the article's Creative Commons licence and your intended use is not permitted by statutory regulation or exceeds the permitted use, you will need to obtain permission directly from the copyright holder. To view a copy of this licence, visit <http://creativecommons.org/licenses/by-nc-nd/4.0/>.

© The Author(s) 2024